Chemical source profiles of fine particles for five different sources in Delhi

Hama, Sarkawt; Kumar, Prashant; Alam, Mohammed S.; Rooney, Daniel J.; Bloss, William J.; Shi, Zongbo; Harrison, Roy M.; Crilley, Leigh R.; Khare, Mukesh; Gupta, Sanjay Kumar

[Link to publication on Research at Birmingham portal](#)

Chemical source profiles of fine particles for five different sources in Delhi

Sarkawt Hama [a], Prashant Kumar [a, b, *], Mohammed S. Alam [c], Daniel J. Rooney [c], William J. Bloss [c], Zongbo Shi [c], Roy M. Harrison [c, f], Leigh R. Crilley [d], Mukesh Khare [e], Sanjay Kumar Gupta [e]

[a] Global Centre for Clean Air Research (GCARE), Department of Civil and Environmental Engineering, Faculty of Engineering and Physical Sciences, University of Surrey, Guildford, GU2 7XH, UK
[b] Department of Civil, Structural & Environmental Engineering, Trinity College Dublin, Dublin, Ireland
[c] School of Geography, Earth and Environmental Sciences, University of Birmingham, Edgbaston, Birmingham, B15 2TT, UK
[d] Department of Chemistry, York University, Toronto, ON, Canada
[e] Department of Civil Engineering, Indian Institute of Technology Delhi, Hauz Khas, New Delhi, 110016, India
[f] Also at: Dept of Environmental Sciences/Center of Excellence in Environmental Research, King Abdulaziz University, Jeddah, Saudi Arabia

HIGHLIGHTS

- Particulate matter profiles are developed for five major air pollutant sources in Delhi.
- Organic matter was most abundant in three combustion profiles (80 −94%).
- Diagnostic ratios (Cl/EC) were highest in solid waste and crop burning.
- Road dust was influenced by anthropogenic sources more than natural.
- OC, Cl, and K were found to be tracers of biomass, solid waste, and crop burning.

GRAPHICAL ABSTRACT
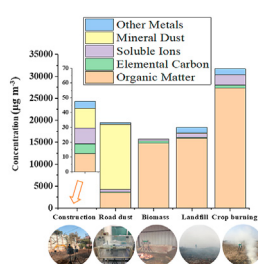
ARTICLE INFO

ABSTRACT

Increasing emissions from sources such as construction and burning of biomass from crop residues, roadside and municipal solid waste have led to a rapid increase in the atmospheric concentrations of fine particulate matter ($\leq$2.5 μm; PM$_{2.5}$) over many Indian cities. Analyses of their chemical profiles are important for receptor models to accurately estimate the contributions from different sources. We have developed chemical source profiles for five important pollutant sources - construction (CON), paved road dust (PRD), roadside biomass burning (RBB), solid waste burning (SWB), and crop residue burning (CPB) - during three intensive campaigns (winter, summer and post-monsoon) in and around Delhi. We obtained chemical characterisations of source profiles incorporating carbonaceous material such as organic carbon (OC) and elemental carbon (EC), water-soluble ions (F$^-$, Cl$^-$, NO$_2^-$, NO$_3^-$, SO$_4^{2-}$, PO$_4^{3-}$, Na$^+$ and NH$_4^+$), and elements (Mg, Al, Si, P, S, Cl, K, Ca, Ti, V, Cr, Mn, Fe, Co, Ni, Cu, Zn, As, Br, Rb, Sr, Ba, and Pb). CON was dominated by the most abundant elements, K, Si, Fe, Al, and Ca. PRD was also dominated by crustal elements, accounting for 91% of the total analysed elements. RBB, SWB and CPB profiles were dominated

* Corresponding author. Global Centre for Clean Air Research (GCARE), Department of Civil and Environmental Engineering, Faculty of Engineering and Physical Sciences, University of Surrey, Guildford, GU2 7XH, UK.
E-mail addresses: P.Kumar@surrey.ac.uk, Prashant.Kumar@cantab.net (P. Kumar).

Megacity Delhi
Source marker

by organic matter, which accounted for 94%, 86.2% and 86% of the total $PM_{2.5}$, respectively. The database of PM emission profiles developed from the sources investigated can be used to assist source apportionment studies for accurate quantification of the causes of air pollution and hence assist governmental bodies in formulating relevant countermeasures.

1. Introduction

Exposure to ambient fine particulate matter ($\leq$2.5 μm; $PM_{2.5}$) is a major threat to human health (Huang et al., 2018; Landrigan et al., 2018), linked to nearly 1.1 million premature mortality cases per year across India (Cohen et al., 2017; Conibear et al., 2018). In particular, the northern region of India suffers the most severe particulate matter air pollution (Guo et al., 2017; Jethva et al., 2018; Kumar et al., 2014; Schnell et al., 2018). The underpinning factors that increase pollution levels include increasing levels of population, industrialisation, urbanisation and energy consumption (Kumar et al., 2013, 2015; Shukla et al., 2020). Delhi currently has a population of 30.29 million (WPR, 2020) with annual average $PM_{2.5}$ concentration levels reaching up to 15-times the WHO guideline of 10 μg m^{-3} (WHO, 2018). $PM_{2.5}$ formed from both natural and anthropogenic sources is considered an important air pollutant, which is responsible for air quality deterioration in cities, such as Delhi (e.g. Kumar et al., 2020). Anthropogenic sources, including transport, industrial processes, power generation, commercial and residential energy use (heating and cooking), diesel generators, construction and road dust emissions contribute to the total ambient concentrations of $PM_{2.5}$ directly (Kumar et al., 2017), and indirectly through gas-to-particle reactions (Hama et al., 2020).

$PM_{2.5}$ can consist of a complex mixture of organic and inorganic chemical constituents (Heal et al., 2012). Chemical composition influences the toxicity of $PM_{2.5}$ (Atkinson et al., 2015), and is associated with emission source and atmospheric physical and chemical processing (Kim et al., 2018). Carbonaceous aerosols and water-soluble ionic species are typically the major components of $PM_{2.5}$, together with trace levels of elements which can be useful for source apportionment. Carbonaceous aerosols consist of organic (OC) and elemental carbon (EC). EC is emitted directly from the incomplete combustion of fossil fuels and biomass. OC can either be emitted directly from sources, such as fossil fuel combustion, traffic emissions and biomass burning (primary organic carbon) or produced via a chemical reaction of its precursor gases and/or their condensation into particles as secondary organic carbon. Inorganic ions in the $PM_{2.5}$ fraction in urban areas occur mainly as ammonium sulphate (($NH_4)_2SO_4$), and ammonium nitrate (NH_4NO_3), originating from the neutralisation of sulfuric acid (H_2SO_4) and nitric acid (HNO_3), respectively, with ammonia in the atmosphere (Squizzato et al., 2013). Metal compounds are also an important part of PM since they can impact human health and the environment (Izhar et al., 2016), and affect heterogeneous chemical processing (SO_2 oxidation). Emission sources of metal elements in $PM_{2.5}$ include a variety of natural and anthropogenic sources, such as crustal and soil dust, construction activities, traffic emissions (exhaust and non-exhaust), industry, municipal waste incineration, and biomass burning (Cheng et al., 2013; Das et al., 2015; Pant and Harrison, 2012). These metals have also been reported to affect numerous cellular oxidation-reduction reactions by influencing key enzymes; an excess of toxic metals in the body can lead to cellular and tissue damage and a variety of adverse impacts on human health (Tchounwou et al., 2012).

An important input to receptor models such as the Chemical Mass Balance (CMB) approach for PM source apportionment is the chemical fingerprint, also referred to as 'source profile', of sources. Source profiles are defined as "fractional mass abundances and uncertainty values of chemical species relative to primary PM emission sources (Watson et al., 2001)"; these are typically produced for different sources, and can be used as input for the CMB apportionment process, and the calculation and validation of emission inventories (Watson et al., 2001). Source profiles used in CMB are typically obtained from direct emission measurements, which do not consider atmospheric processing (Pernigotti et al., 2016). Further, previous studies have suggested that the lack of location/region-specific source profiles in India (Table 1), severely limits the ability of receptor models to apportion sources correctly (Pant and Harrison, 2012). Thus, locally derived aerosol source profiles are vital for source apportionment models.

Limited studies have reported PM source profiles in India (Table 1). To date, no studies have reported the source profiles of $PM_{2.5}$ in Delhi in detail. Therefore, this work develops an in-depth understanding of profiles for important PM diffused sources in Delhi, based upon direct real-world sampling, and establishes a PM emission profile database that can assist source apportionment studies and allow governmental bodies to formulate relevant countermeasures. The objective of this work is thus to characterise the chemical composition of PM for five different major sources in Delhi, evaluate the similarities and differences among the profiles, and reconstruct mass closures using measured species, calculated enrichment factors and source signatures of PM.

2. Materials and methods

2.1. Sampling sites

In order to develop profiles of major pollutant sources in and outside Delhi (Supplementary Information, SI, Section S1), we selected specific sampling locations (Fig. 1) for each of the five sources considered (Table 2), as discussed below:

- **Construction (CON)**: Samples were collected at the Indian Institute of Technology Delhi (IITD, 28.32 N, 77.11E) campus. Sampling was carried out for 8 h (1000−1800h; local time) when construction activity was ongoing. During the sampling period, the construction site was at the initial phase of substructure construction when groundwork activities such as the excavation, filling and soil cutting activities were in progress.
- **Paved road dust (PRD)**: Samples were collected on the main road (inside IITD, 28.32 N, 77.11E); Ring road (outside IITD, 28.33 N, 77.11E); Mathura Road at the Central Road Research Institute (CRRI, 28.33 N, 77.16E); and Okhla area (28.33 N, 77.17E). Dust samples were collected from paved roads at the above locations; further details are given in Section 2.2. Sampling was carried out for 30 min periods (ensuring adequate PM mass was collected on the filter in the resuspension chamber (Fig. S1).
- **Roadside biomass burning (RBB)**: Samples were collected within the IITD campus (28.32 N, 77.11E), where people used

Table 1
Summary of previous studies on PM source profiles in India.

City	Measurement years	Type of source profiles	Author (year)
Raipur	unknown	Domestic cooking, solid waste burning and industrial process	Bano et al. (2018)
Bhopal	unknown	Paved road, unpaved road dust	Samiksha et al. (2017)
Raipur	unknown	Traffic and Dust	Matawle et al. (2015)
Delhi	2012 and 2013	Soil and road dust, brake pad	Pant et al. (2015)
Raipur	unknown	Industrial furnaces, household fuel burning, solid waste burning, welding workshop burning,	Matawle et al. (2014)
Nagpur	2009 and 2010	Residential, and industrial	Pipalatkar et al. (2014)
Bengaluru, Chennai, Delhi, Kanpur, Mumbai and Pune	Unknown	Soil dust, paved road and unpaved road dust, coal and wood combustion in stoves, waste burning, fuel oil combustion, agricultural waste burning, brick kiln.	Patil et al. (2013)

Fig. 1. Map showing the location of all source profile sampling sites. Blue dots represent the location of the sampling. All the sampling was carried out within Delhi, except for crop residue burning that took place in Panipat. The light green area represents Delhi, and the purple area represents the Haryana state. (For interpretation of the references to colour in this figure legend, the reader is referred to the Web version of this article.)

Table 2
Description of sites, number of filters, and their locations used for PM source profiles. Period of sampling (winter: 18th January- 8th February 2018; Summer: April 2018; autumn: October 2018) for each filter was 30 min for all source profiles, except CON, for which samples were collected for 8 h. Note that PM_{10} samples were only collected for PRD profile, and $PM_{2.5}$ samples for all the other profiles.

Source profiles (code)	Description and location of sites	Number of collected PM filters		
		Winter	Summer	Autumn
Construction (CON)	Residential and commercial, inside the IIT Delhi campus	6	—	—
Paved Road dust (PRD)	IIT main Road (inside IIT Delhi Campus), Ring-road (outside the IIT Delhi campus), Mathura Road (at the CRRI), and Okhla area	10	10	—
Roadside biomass burning (RBB)	Residential, inside the IIT Delhi	12	—	—
Solid waste burning (SWB)	Solid waste open areas (Bhalswa outside Delhi)	6	12	
Crop residue burning (CPB)	Agricultural waste burning areas in Panipat	—	—	16

biomass for cooking in the evening. Again, sampling was carried out for 30 min periods at the site.

- **Solid waste burning (SWB)**: Sampling was carried out for 30 min periods at the Bhalswa open waste burning site (28.45 N, 77.09E) which is located at around 11 km northwest of Delhi.
- **Crop residue burning (CPB)**: Samples were collected for 30 min periods in Panipat city (28.23 N, 76.57E) as rice crop residue burning is popular after harvesting practices performed by farmers in October and November in the states of Punjab and Haryana despite legislation in place to control this (Kaskaoutis et al., 2014).

2.2. Sampling

PM samples were collected during winter (January–February 2018), summer (April 2018), and post-monsoon seasons (October 2018) (Table 2). Two Mini-Vol portable air samplers (AirMetrics, M.T., 2006), equipped with a $PM_{2.5}$ impactor sampling with a flow rate of 5 L min^{-1}, were simultaneously located close to the sources at each site (in-line with wind direction and directly into the source dominated volume). It is worth noting that the wind speed during the sampling duration was consistently low (<1 m s^{-1}; Fig. S2) and thus the influence of the meteorological conditions on the measured concentrations can be expected to be negligible. Following the US EPA protocols for PM collection on filters (Chow and Watson, 1998), a total of 72 filter samples (52 of $PM_{2.5}$, and 20 of PM_{10}, Table 2) were sequentially collected, which included 36 samples on 47 mm Quartz filters and the same number on 47 mm Teflon filters. We calculated PM mass concentrations from the mass collected on each filter by the samplers gravimetrically. Paved road dust sampling followed procedures reported in previous studies (Kong et al., 2012; Patil et al., 2013). Paved road dust samples were collected by sweeping 0.5–1 kg of the dust using a clean plastic dustpan and brush from the surface and storing in zipped polyethylene bags. Samples were dried, sieved (Tyler 400-mesh screen) by using the method described by Matawle et al. (2015), and mechanically re-suspended in a laboratory chamber (Fig. S1) and sampled through PM_{10} inlets at an average flow rate of 5 L min^{-1}. The sampler was mounted at the bottom of the resuspension chamber to collect PM_{10} samples on the quartz and Teflon filters separately.

2.3. Chemical analysis

All the filter samples were analysed for three types of chemical species: (i) carbonaceous material including OC and EC (including 8 sub-fractions); (ii) 8 water-soluble ions (F^-, Cl^-, NO_2^-, NO_3^-, SO_4^{2-}, PO_4^{3-}, Na^+ and NH_4^+); and (iii) 23 elements (Mg, Al, Si, P, S, Cl, K, Ca, Ti, V, Cr, Mn, Fe, Co, Ni, Cu, Zn, As, Br, Rb, Sr, Ba, and Pb). OC and EC concentrations were determined using the DRI Model 2015 Multi-wavelength Thermal/Optical Carbon Analyser utilising the EUSAAR2 (European Supersites for Atmospheric Aerosol Research) protocol (Cavalli et al., 2010). The carbonaceous material collected was exposed to different thermal conditions, so that the samples were thermally desorbed from the filter medium under an oxygen-free inert helium atmosphere, followed by an oxidising atmosphere containing an oxygen/helium mixture. Firstly, OC was vaporised in an inert atmosphere, and then EC was converted into vapour upon exposure to a higher temperature and an oxidation atmosphere of 98%He and 2%O_2. Quartz filters were analysed for eight individual carbon fractions, OC1, OC2, OC3 and OC4 at 200, 300, 450 and 650 °C, respectively. EC1, EC2, EC3 and EC4 were obtained at 500, 550, 700, and 850 °C, respectively (Table S1). After extraction of a fraction of the samples in ultra-pure water, chromatography (Thermo Dionex; Sunnyvale, CA) was used for analysing quartz filters for ionic species. The Teflon filters were analysed for

elements from Na to Bi using energy dispersive X-ray fluorescence (ED-XRF) (PANalytical Epsilon 5), which was calibrated using MicroMatter thin-film standards (Watson et al., 1999).

2.4. Quality control and assurance

Prior to sampling, quartz filters were baked at 550 °C for 12 h to remove any artefacts present. Teflon filters were equilibrated and desiccated at a temperature of 20–25 °C and RH of 40–50% in a controlled room before gravimetric analysis; they were weighed before and after sampling using a microbalance (Sartorius CPA2P–F) with a sensitivity of ±1 μg. After sampling, the filters were sealed in aluminium foil bags and stored in a freezer (−20 °C) prior to analysis. All analytical procedures were performed in line with strict quality control (QC) and quality assurance (QA) measures. The method detection limits (MDL) for ions were in the range 0.004 μg mL^{-1} to 0.533 μg mL^{-1}. The MDL for elements analysed by XRF ranged from 1.3 ng cm^{-2} to 180.3 ng cm^{-2}, and the MDL for OC and EC was 2.7 and 0.1 μg cm^{-2}, respectively. The measurement for each sample was subtracted from the ambient values to obtain the final result which represented the real profile for each source. The concentrations of all species near to source and in ambient condition are summarised in Table S2. These values indicate that the source profiles are not highly affected by ambient concentration (The ambient correction was <2% for all profiles except CON). In order to develop the understanding of the local ambient concentrations around the monitoring sites, source profile measurements were carried out simultaneously both at the upwind and downwind of each site. All source profile samples were corrected by subtracting these upwind measurements of local ambient conditions during the measurements. CON profile was an exception since the site area was large and upwind measurements were not possible. An approach to identify and subtract ambient background concentrations for the CON sample is summarised in SI Section S2.

2.5. Chemical mass closure

PM mass reconstruction was performed by taking the sum of mineral dust (MD), organic matter (OM), elemental carbon (EC), inorganic soluble ions, and other metals (except mineral dust metals). The mineral dust (i.e. soil, dust, or mineral) was estimated using Eq. (1):

$$MD = 2.49 \times Si + 2.2 \times Al + 1.94 \times Ti + 1.48 \times Fe + 1.40 \times Ca + 1.67 \times Mg \tag{1}$$

where the numbers correspond to mass adjustment for the principal oxides (SiO2, Al2O3, TiO2, FeO/Fe2O3, CaO, MgO) of the elements quantified (Chan et al., 1997; Marzaccan et al., 2001). OM was calculated as 1.6×OC (Chow et al., 2015) to express the hydrogen, oxygen, and other elements present in the ambient organic aerosol. OM is estimated from an organic carbon (OC) multiplier that can range from 1.2 to 1.8, based on of OM oxidation and secondary organic aerosol formation (Chow et al., 2015). Since we focus on more than one source here, we used 1.6 (for CON, RBB, SWB, and CPB) and 1.2 (for PRD) in our case to obtain better mass closure. The EC contribution was reported as analysed by the Thermal Optical Method (Section 2.3).

The inorganic water-soluble ions contribution was calculated as the sum of concentrations of all anions and cations (Eq. (2)), which have a significant contribution to each source profiles as follows:

$$\text{Ions} = \left[SO_4^{2-}\right] + \left[NO_{2-}\right] + \left[NO_{3-}\right] + \left[Cl^-\right] + \left[F^-\right] + \left[PO_4^{3-}\right]$$
$$+ \left[Na^+\right] + \left[NH_4^+\right] \tag{2}$$

Trace elements represent a small percentage of total PM mass concentrations. However, they have a significant impact on human health (Moreno et al., 2004) and the environment, owing to their toxicity and anthropogenic origin (Rees et al., 2004). We estimated the contribution of trace elements by summation of all other metals, except those used in Eq. (1).

2.6. Enrichment factors

Enrichment factors (EFs) are concentrations of elements normalised as ratios to another constituent present. In order to further understand the sources of the elements (crustal versus anthropogenic), EFs were calculated for crustal elements in CON and PRD using Eq. (1) based on continental crust concentrations using Al is the reference element (Pant et al., 2015; Crilley et al., 2017; Hama et al., 2018). Al is used as a reference element due to its high relative abundances in the earth-crust and soil (Cesari et al., 2012) and its conventional use for this purpose. The crustal composition given by Wedepohl (1995), the EFs were calculated using Eq. (3):

$$EF_X = (C_X/C_{Al}) \text{ sample}/ (C_X/C_{Al}) \text{ crustal} \tag{3}$$

where C_X and C_{Al} represent the mass concentrations of element and aluminium (Al) in the sample and upper continental crust, respectively. EFs were calculated based on the upper continental crust composition (Hama et al., 2018). EF values > 1 typically indicate enrichment of the sample by anthropogenic sources.

2.7. Calculation of source marker

Source markers of PM are mostly described by a specific size distribution, suite of elements and ratios of chemical compounds, elements or isotopes (Mitra et al., 2002). To further understand the sources of the different chemical species, relative source signatures were calculated for all developed source profiles by the following equation (Yang et al., 2002; Kong et al., 2012):

$$Ratio_{i,j} = \frac{(Xi/\Sigma X)j}{(Xi/\Sigma X)min} \tag{4}$$

where Xi is the ith individual chemical species concentration for each profile; $(Xi/\Sigma X)j$ is the quotient of the ith individual species divided by the sum of 39 chemical species concentrations for source j; $(Xi/\Sigma X)min$ is the minimum quotient of the ith individual species divided by the sum of 39 chemical species concentrations (Chen et al., 2003; Yang et al., 2002). In addition, normalisation was applied according to Mitra et al. (2002) and Kong et al. (2012) to minimise the effect of physical parameters and decrease variation between all the chemical species. Normalised individual chemical species concentrations were calculated by dividing the ith individual chemical species concentration by the sum of ith individual species concentration for all the source profiles (Kong et al., 2012).

3. Results

Table 3 shows the composite profiles of measured chemical species; their standard deviations (SD) were calculated to indicate the representative distributions of chemical abundances and their variabilities (Watson et al., 2001). Organic aerosols accounted for a significant fraction of PM mass in all five sources, accounting for

~94%, 86%, 86.2%, 26% and ~18% of $PM_{2.5}$ mass for RBB, CPB, SWB, CON and PRD, respectively. The highest percentage of carbonaceous materials were found in combustion source profiles (SWB, RBB, and CPB). In CON, after the carbonaceous species, K (12.1 ± 9.3%), Si (11.5 ± 8.9%) and Na^+ (7.3 ± 2.9%) showed the highest percentage among other species. In PRD, Si (13.1 ± 2.1%), Ca (11.2 ± 1.4%) and Al (6.1 ± 0.9%) showed the highest fractions when compared with other species. This is consistent with a previous study for different Indian regions in which they found the highest percentages of Si, Ca, and Al (~40%) in a similar source profile study (Patil et al., 2013; Matawle et al., 2015). Interestingly, we observed the highest percentages for Cl (SWB: 7.1 ± 2.6%; CPB: 4.8 ± 1.8%; RBB: 0.5 ± 0.4%) in source profiles of combustion sources (RBB, SWB, and CPB). The above findings and these abundances are comparable to those from previous studies (Bano et al., 2018; Ni et al., 2017; Sun et al., 2019b), which also found a similar proportion for Cl^-, 0.4 ± 0.2% for RBB and ~6.4 ± 4.4% for CPB profiles. The profiles for individual sources are discussed in detail in the following sub-sections.

3.1. Construction

Fig. 2 shows the variation of mass concentration of chemical species in the CON source profile. Table S4 summarises the mean, SD and median values of OC, EC and their fractions for the CON profile. OC and EC concentrations were 7.7 ± 5.9 and 6.5 ± 0.15 µg m^{-3}, respectively. In addition, OC and EC fractions, OC4 (4.6 ± 0.5 µg m^{-3}) and EC4 (3.8 ± 0.4 µg m^{-3}), were relatively higher than OC3 (2.7 ± 0.8 µg m^{-3}) and EC3 (3.0 ± 0.8 µg m^{-3}) (Table S4). The OC (13%) and EC (18%) levels were higher in our CON profile than those reported by Patil et al. (2013) who found lower OC (~9%) and EC (~1%). This may be as a result of the sampling method used and the analysis protocol applied to the samples. For example, we followed the EUSAAR protocol as opposed to the IMPROVE (Interagency Monitoring of Protected Visual Environment) protocol used by Patil et al. (2013) for OC and EC determination. In addition, Na^+ (4.1 ± 0.5 µg m^{-3}), NO_3^- (3.9 ± 1.6 µg m^{-3}) and SO_4^{2-} (1.5 ± 1.1 µg m^{-3}) were the dominant ions (Fig. 2; Table S4) found. CON dust is mainly a mixture of construction materials such as cement, grit, and sand, alongside soil and road dust. CON profile was found to be dominated by Na^+, NO_3^- and SO_4^{2-} which are characteristic of cement dust emissions (Yatkin and Bayram, 2008). In previous studies, SO_4^{2-} and Ca were found to be dominant for the CON profile (Patil et al., 2013; Sun et al., 2019a). The most abundant elements were K, Si, Ca, Al, Fe and Mg in CON which accounted for 84% of the total analysed elements. The crustal elements Si, Fe, Al, and Ca may be attributed to activities such as aggregate processing and geological dust. This is consistent with earlier studies reporting construction profile studies (Chen et al., 2017; Patil et al., 2013) with high proportions of crustal elements (~85% of the total analysed elements) in India, and (~88% of the total analysed elements) in China. The trace and heavy elements Cr, Mn, Cu, Zn, As, and Pb, found relatively lower fractions and accounted for 6% of the total analysed elements. These elements play a key role in atmospheric pollution impact on human health (Meng et al., 2013). The above observations allow us to conclude that the CON profile was dominated by OC, EC, Na^+, NO_3^- and SO_4^{2-}, and the most abundant elements were K, Si, Fe, Al, and Ca.

3.2. Paved road dust

Paved road dust is one of the major sources of particulate matter (particularly PM_{10}) in Delhi (Patil et al., 2013). Road dust consists primarily of coarse-sized particles derived from different sources such as vehicular emissions, brake and tyre wear and mineralogical dust (Pant and Harrison, 2013). It is interesting to observe that the

Table 3
Composite PM source profiles in percent weight by the mass of emissions from studied sources. We averaged concentrations of profiles collected over the two different seasons Session-specific profiles are presented in SI Table S3. Note that 'BDL' denotes below the detection limit.

Species	Source type (percent weight by mass)				
	CON	PRD	RBB	SWB	CPB
OC	12.9 ± 6.4	15.1 ± 4.3	58.7 ± 7.0	53.8 ± 5.8	53.7 ± 4.7
EC	17.9 ± 9.3	0.9 ± 0.2	5.7 ± 3.7	2.0 ± 1.8	3.5 ± 0.9
F^-	BDL	BDL	0.2 ± 0.1	BDL	0.2 ± 0.1
Cl^-	BDL	0.3 ± 0.2	0.2 ± 0.1	6.0 ± 3.2	4.0 ± 2.1
NO_2^-	2.1 ± 1.7	BDL	0.6 ± 0.4	BDL	0.4 ± 0.06
SO_4^{2-}	6.9 ± 5.0	0.8 ± 0.6	0.7 ± 0.1	0.9 ± 0.7	1.1 ± 0.9
NO_3^-	8.7 ± 1.3	0.3 ± 0.2	0.2 ± 0.2	BDL	0.1 ± 0.01
PO_4^{3-}	1.6 ± 1.1	1.5 ± 1.4	0.6 ± 0.4	12.7 ± 10.3	2.0 ± 0.5
Na^+	7.3 ± 2.9	0.5 ± 0.4	0.2 ± 0.1	2.2 ± 2.0	0.6 ± 0.5
NH_4^+	BDL	0.04 ± 0.03	0.6 ± 0.5	15.1 ± 14.0	0.9 ± 0.3
K^+	0.2 ± 0.1	0.2 ± 0.1	0.08 ± 0.03	0.2 ± 0.1	1.4 ± 0.5
Mg	0.5 ± 0.4	1.4 ± 0.2	BDL	BDL	BDL
Al	4.5 ± 0.9	6.1 ± 0.9	0.014 ± 0.01	0.1 ± 0.05	BDL
Si	11.5 ± 8.9	13.1 ± 2.1	BDL	0.7 ± 0.6	BDL
P	1.03 ± 0.9	0.5 ± 0.1	0.009 ± 0.003	0.04 ± 0.03	0.02 ± 0.005
S	1.8 ± 0.2	0.6 ± 0.1	0.12 ± 0.08	0.6 ± 0.5	0.3 ± 0.06
Cl	1.4 ± 1.0	0.3 ± 0.1	0.5 ± 0.4	7.1 ± 2.6	4.8 ± 1.8
K	12.1 ± 9.3	2.1 ± 0.2	0.13 ± 0.07	0.3 ± 0.1	1.7 ± 0.8
Ca	6.4 ± 0.9	11.2 ± 1.4	0.021 ± 0.019	0.03 ± 0.02	BDL
Ti	0.2 ± 0.01	0.6 ± 0.05	0.003 ± 0.001	BDL	BDL
V	BDL	0.01 ± 0.001	BDL	BDL	BDL
Cr	0.03 ± 0.02	0.03 ± 0.009	BDL	BDL	BDL
Mn	0.3 ± 0.2	0.1 ± 0.007	0.001 ± 0.0009	0.0005 ± 0.0001	0.002 ± 0.001
Fe	4.3 ± 1.3	6.1 ± 0.5	0.009 ± 0.008	0.02 ± 0.01	0.03 ± 0.02
Ni	BDL	0.006 ± 0.0005	BDL	0.07 ± 0.04	BDL
Cu	0.1 ± 0.09	0.05 ± 0.01	0.001 ± 0.001	0.02 ± 0.01	BDL
Zn	2.4 ± 1.0	0.1 ± 0.03	0.005 ± 0.004	0.02 ± 0.01	0.02 ± 0.01
As	0.1 ± 0.09	0.004 ± 0.0006	0.003 ± 0.002	BDL	BDL
Br	BDL	0.002 ± 0.0007	0.002 ± 0.001	0.02 ± 0.01	0.03 ± 0.01
Rb	BDL	0.02 ± 0.001	BDL	0.002 ± 0.001	0.003 ± 0.001
Sr	BDL	0.06 ± 0.007	BDL	0.002 ± 0.0007	BDL
Ba	BDL	0.06 ± 0.02	BDL	BDL	BDL
Pb	BDL	0.02 ± 0.005	0.002 ± 0.0007	0.02 ± 0.01	0.005 ± 0.002

carbonaceous species and their fractions in PRD were dominated by OC (2937.9 ± 1583.3 μg m^{-3}), OC4 (1351.0 ± 651.3 μg m^{-3}), OC3 (726.3 ± 431.6 μg m^{-3}) and EC1 (303.8 ± 228.8 μg m^{-3}) (Table S5). The abundance of EC and OC in the PRD profile may be as a result of traffic emissions including brake and tyre wear and oil drips as reported by Ho et al. (2003). Previous source profile studies in India reported similar results (Patil et al., 2013; Samiksha et al., 2017). A study in China (Chen et al., 2017) found lower levels of OC and EC in the road dust profiles, which may be due to the different chemical composition of road materials in Chinese cities. The PRD profiles developed in the present study were observed to have high levels of water-soluble ions such as PO_4^{3-} (198.2 ± 175.4 μg m^{-3}), SO_4^{2-} (126.4 ± 96.4 μg m^{-3}) and Na$^+$ (76.5 ± 57.0 μgm^{-3}). Interestingly, SO_4^{2-} was found to be abundant, accounting for 23.3% of the total water-soluble ion content in PRD. This may be associated with the chemical reactions of secondary aerosols with crustal elements (for example, calcium); this is consistent with previous studies (Patil et al., 2013; Pervez et al., 2018; Sun et al., 2019a), which also found high levels of SO_4^{2-} (10−20% of total ions) in road dust profiles. In addition, the elemental composition of PRD is dominated by crustal elements such as Si, Ca, Al, K, Fe, Ti and Mg (Table S5, Fig. 3). The crustal elements accounted for 91% of the total analysed elements. Si and Ca showed the highest fraction in PRD which accounted for 30%, and 27% of the total elements, respectively (Table S5). A spill of building materials such as the cement, sand or mixture of such materials on the construction site (Yu et al., 2020) are expected on the construction sites as an important source of PM. Such processes contribute more to coarse fraction of PM compared with their smaller counterparts. Ca has been widely used as a marker for crustal dust and construction activity (Pant and Harrison, 2013). In Delhi, a higher abundance of Ca-rich dust is attributed to the dust from the Thar Desert (Pant et al., 2015). Si and Ca were comparable and dominant, reflecting combined effects of building materials and soil dust (Chen et al., 2017). The proportions of Si and Ca is in line with those reported in Matawle et al. (2015) and Samiksha et al. (2017), who found high crustal fractions 43.5−83.8% in Raipur city, India, and Si (~17%) and Ca (~6.5%) of PM$_{10}$ mass in Bhopal, India, respectively. It is interesting to note that the crustal road dust fractions show differences between this study and previous work, with the proportions of crustal elements found here being consistently much higher than the above cities. Road dust composition may vary with location, and so obtaining such different source profiles is plausible, and highlights the importance of making regionally localised measurements. In order to explore the origins of these crustal elements in both CON and PRD profiles, we calculated their enrichment factors (Section 4.2). The other elements accounted for only 4.3% of the total elements. Of these, the PM$_{10}$ profiles for PRD were found to have notable levels of Pb (3.2 ± 1.6 μg m^{-3}). Most Indian cities, including Delhi, phased out leaded petrol after the year 2000 (Singh and Singh, 2006). Since Pb is still persistent in road dust samples implies that this is likely to be due to anthropogenic sources such as coal burning and possibly brake dust (Xu et al., 2012; Zhang et al., 2014) and ongoing emission of Pb from industrial activities, etc (Shen et al., 2016). PRD was dominated by OC, with major OC fractions being OC4 and OC3. We also found high levels of water-soluble ions such as PO_4^{3-}, SO_4^{2-}, and Na$^+$. Overall, PRD was dominated by crustal elements which accounted for 91% of the total analysed elements. Si and Ca showed the highest fractions in PRD, which accounted for 30%, and 27% of total elements in road dust, respectively.
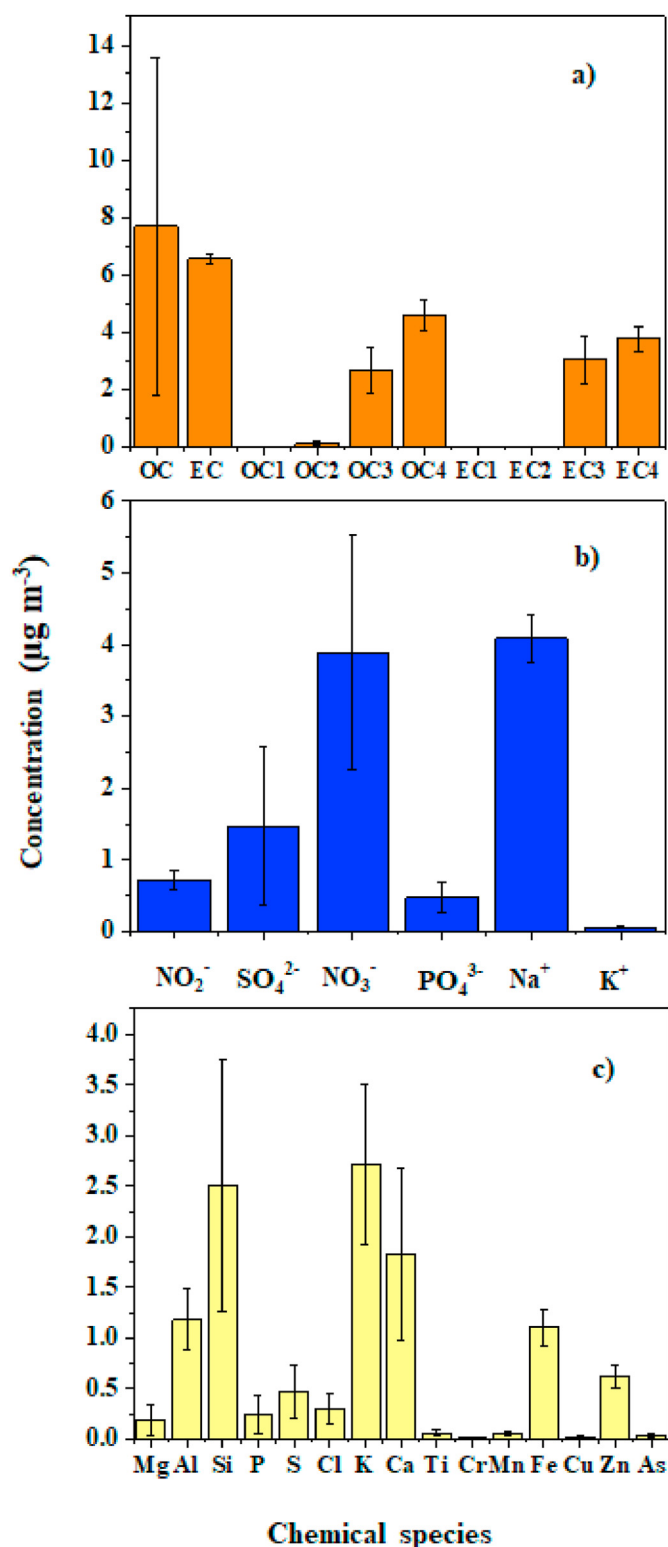
Fig. 2. Variability in mass concentrations ($\mu g \, m^{-3}$) of (a) carbonaceous species, (b) ions, and (c) elements for construction profile. The error bars represent the standard deviation for each of the species.

Fig. 3. Variability in mass concentrations ($\mu g \, m^{-3}$) of (a) carbonaceous species, (b) ions, and (c) elements for paved road dust profile. The error bars represent the standard deviation for each of the species.

3.3. Roadside biomass burning

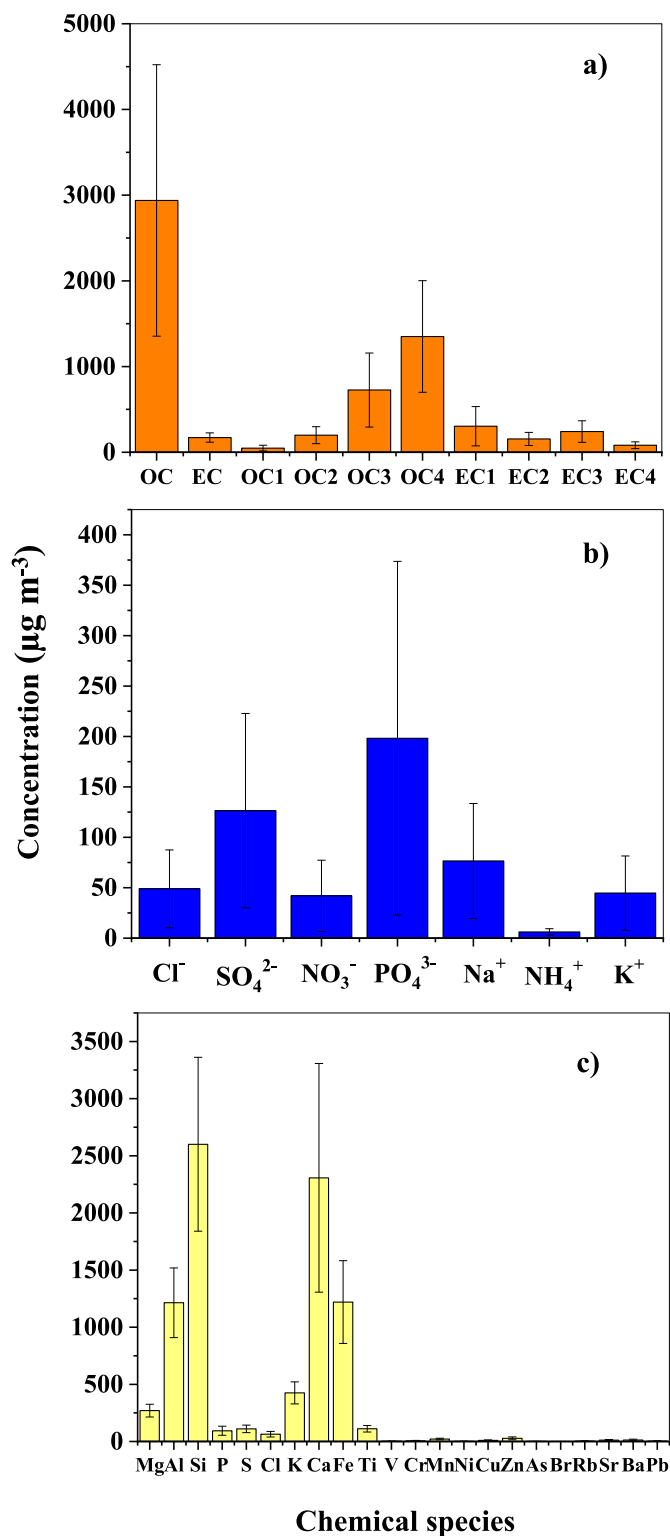Despite the ban on RBB, it can still commonly be seen across Delhi during the winter for heating and cooking purposes. This is mostly due to the inefficient collection of roadside waste such as the dried leaves, papers, plastics, or clothes that results in accumulating over a period and is generally burned by the local people as an easy way of clearing it up. The RBB samples collected were dominated by OC ($9265.3 \pm 5207.7 \, \mu g \, m^{-3}$). Previous studies

reported that combustion and biomass burning are major sources of organic carbon (Denier van der Gon et al., 2015; Gao et al., 2018; Vicente and Alves, 2018). Diagnostic ratios of chemical species can be used as source indicators (Ni et al., 2017; Sun et al., 2019b). The OC/EC ratio is often applied to distinguish between combustion sources (Han et al., 2016), with (lower temperature) biomass burning associated with higher OC/EC ratios than coal combustion and vehicle exhaust (Chen et al., 2015). The OC/EC ratios found in RBB (16.9 ± 6.7), were higher than those reported by Matawle et al. (2014) in Raipur, India and by Zhang et al. (2012) in Guizhou, China, who found lower OC/EC ratios of 6.9 and 10.7 for domestic wood burning. Our results suggest that OC was dominated by primary organic aerosol in the RBB profile. It can be inferred from the wood emissions that OC/EC ratios vary considerably, probably because of variation in the nature of the fuel, the combustion process (temperature, oxygen supply, fuel moisture level) sampling treatment or the analysis protocol – hence the approach adopted here of real-world sampling *in situ*. Interestingly, the different values of OC/EC in RBB between the present and the above studies may be due to different sampling methods used; Matawle et al. (2014) and Zhang et al. (2012) adopted laboratory-scale studies indoors, whereas the present study adopted real-world sampling on open-air wood burners. The major ions were SO_4^{2-} (74.3 ± 32.7 µg m^{-3}), NO_2^- (66.5 ± 54.2 µg m^{-3}), PO_4^{3-} (60.1 ± 44.9 µg m^{-3}), and Cl^- (24.1 ± 11.9 µg m^{-3}) (Table S6, Fig. 4). Biomass burning emitted five major ions including K^+, SO_4^{2-}, NH_4^+, Cl^-, and NO_2^- (Thepnuan et al., 2019). In the present study, the K^+/K ratio was 0.66, which is consistent with previous studies (Patil et al., 2013; Watson and Chow, 2001), reporting comparable K^+/K ratio values, of 0.68 and 0.8, respectively. As expected, the most abundant elements from biomass burning were Cl, S, and K, which accounted for 88% of the total elements (Table S6). The abundance of tracers such as, K, Cl and S confirms this source to be that of biomass burning. In fact, K is globally considered as a biomass marker (Pant and Harrison, 2012; Jain et al., 2020). Crustal elements (Si, Mg, and Na) were not found in the RBB profile. Relatively lower proportions of the other elements were found, for 11% of the total elements present. Overall, RBB was dominated by OC which accounted for 58.7% of $PM_{2.5}$ mass. The main ions found in the RBB profile were SO_4^{2-}, NO_2^-, PO_4^{3-} and Cl^-. The most abundant metals found were Cl, S and K which accounted for 88% of the total elements.

3.4. Solid waste burning

Open burning of municipal solid waste is an important contributor to $PM_{2.5}$ in Delhi and other Indian cities (Patil et al., 2013). OC was found to be the most abundant species (9940.8 ± 5812.8 µg m^{-3}). The OC/EC ratio of 43.7 and a K^+/K ratio of 0.86, were higher than those reported in the previous study (OC/EC = 19.4, and K^+/K = 0.69) for solid waste burning in India (Bano et al., 2018). The reason for higher ratios may be due to different sampling methods and site locations. In addition, another reason may be due to the type of waste generated and burnt. While it was not feasible to characterise the waste burned in detail, various types of solid waste material such as plastics, glass, paper, rubber, clothes, cardboard and packaging material can be expected to be burned at the site (Malav et al., 2020). OC/EC ratios also depend on the analysis protocol applied to the collected samples (Chow et al., 2004; Han et al., 2016). Our results suggest that primary organic aerosol also contributed to the OC in the SWB profile. SWB was dominated by Cl^-, NH_4^+, and PO_4^{3-} ions which accounted for 48%, 20% and 16% of total analysed ions, respectively (Table S7, Fig. 5). Previous studies have reported similar profiles for SWB (Bano et al., 2018; Matawle et al., 2014; Patil et al., 2013). In addition, the ratios given in Table S7 are known to be tracers of open solid waste and
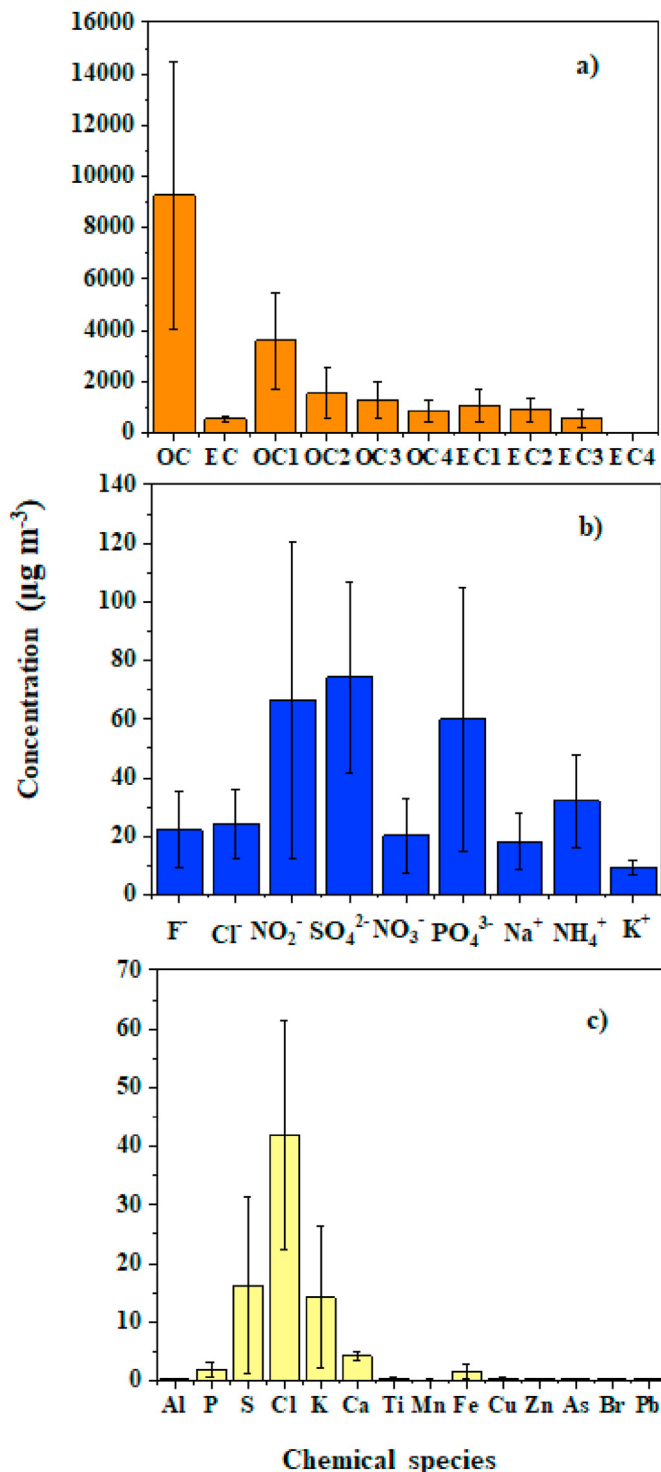

Fig. 4. Variability in mass concentrations (µg m^{-3}) of (a) carbonaceous species, (b) ions, and (c) elements for roadside biomass burning profile. The error bars represent the standard deviation for each of the species.

biomass combustion emissions. SWB's K/EC ratio (0.07) was higher than RBB' K/EC ratio (0.03), but lower than CPB's K/EC ratio (0.5). It is interesting to note that the Cl/EC ratio (5.7) for the SWB profile was the highest (Table S7), which was 3–4 times higher than the reported values for crop residue burning (1.1–1.3). The ratio K/OC was found to be similar to that in the RBB profile, but lower (15–20 times) than the CPB profile (Table S7). This might be linked to the
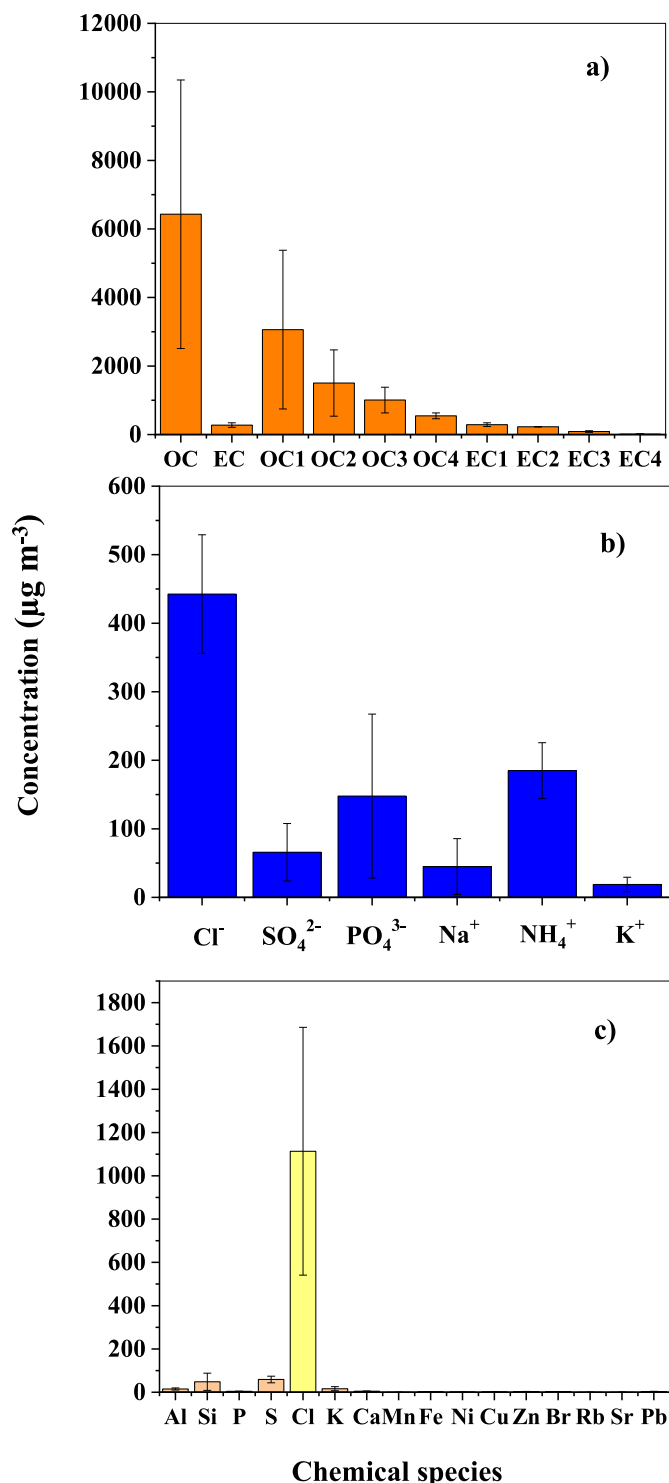
Fig. 5. Variability in mass concentrations ($\mu g\ m^{-3}$) of (a) carbonaceous species, (b) ions, and (c) elements for solid waste burning profile. The error bars represent the standard deviation for each of the species.

1.3%, of total measured elements, respectively (Table S8). Interestingly, Zn ($2.9 \pm 0.7\ \mu g\ m^{-3}$) and Pb ($2.5 \pm 1.8\ \mu g\ m^{-3}$) showed the highest mass concentrations among other trace elements (Table S8). This is consistent with previous source profile studies (Bano et al., 2018; Matawle et al., 2014), reporting similar levels of Zn and Pb in SWB profiles in India. Zn and Pb are also linked to waste incineration (Duan and Tan, 2013). Rai et al. (2020) found a strong correlation between Zn and Pb in waste incineration in Delhi, thus supporting the high concentrations for Zn and Pb found in our case for the SWB. It can be concluded that the OC was the most abundant species and accounted for 53.8% of measured $PM_{2.5}$ mass. OC1 showed the highest, followed by OC2, OC3, and OC4. EC1 showed the highest, followed by EC2, EC3, and EC4, indicating that biomass burning had the highest contribution in the SWB. The Cl/EC ratio for the SWB profile was the highest among all other diagnostic ratios, suggesting these two ratios (Cl/OC and Cl/EC) may be used as a source indicator for the SWB source profile. The elemental composition of the SWB was dominated by Cl, S, and K.

3.5. Crop residue burning

Burning of crop residue in agricultural fields leads to emissions of various air pollutants, which can play a dominant role in atmospheric composition locally, and regionally (Ravindra et al., 2019). OC is a major species in the CPB source profile ($17053.2 \pm 6145.1\ \mu g$ m-3). OC1 and OC4 showed the highest ($6427.9 \pm 2945.1\ \mu g\ m^{-3}$) and the lowest ($1452.5 \pm 205.4\ \mu g\ m^{-3}$) contributions (Table S9). EC concentrations were $700.6 \pm 50.3\ \mu g\ m^{-3}$, with the highest and lowest EC fraction for EC1 ($1984.7 \pm 443.3\ \mu g\ m^{-3}$) and EC4 ($47.3 \pm 21.4\ \mu g\ m^{-3}$), respectively. This result suggests that these fractions have different emission sources. For example, OC1 represents the biomass burning contribution. The OC/EC ratio of 24.3 is higher for crop residue burning than other sources (construction (2.5), road dust (18.8)). This suggests that primary organic aerosol in the CPB profile contributed to the OC. In addition, major ions were Cl^- ($772.7 \pm 201.4\ \mu g\ m^{-3}$), PO_4^{3-} ($452.8 \pm 13.2\ \mu g\ m^{-3}$) and K^+ ($253.8 \pm 74.8\ \mu g\ m^{-3}$). Cl^- and K^+, which have been reported in previous source apportionment studies (Wang et al., 2020a; Kumar and Raman, 2020), are often used as tracers for crop residue burning emissions. Harvesting followed by the burning of the crop residue in the field during the post-monsoon season in the region of Haryana is common practice since it is an easy and economical way of coping with large quantities of crop residues; this could be one reason why Cl^- PO_4^{3-} and K^+ are found in the Delhi atmosphere. In addition, K is mostly water-soluble, as indicated by the K^+/K ratio, the value was 0.74 in this study for the CPB profile. This is in agreement with results reported in Ni et al. (2017), who also found a very similar K^+/K ratio of 0.77. Watson et al. (2001) also reported ratios of K^+/K ratios ranging from 0.1 in geological material to 0.9 in vegetative burning profiles (such as crop residue). Table S9 shows the source diagnostic ratios for the CPB profile. These ratios have been adopted in the literature to assess biomass burning contributions (Sun et al., 2019b). It is interesting to note that the K/EC ratios (Table S7) showed comparable values with those reported in Sun et al. (2019b), while they were lower than those measured in laboratory chamber experiments (Ni et al., 2017) values of 0.4 and 2.26, respectively. Thus, the diagnostic source ratios and K found in our studies can be used as good source markers for crop residue burning profiles. Other ratios for the CPB source (Table S7) were largely comparable with RBB and SWB profiles. However, the Cl/EC (1.3, Table S7) ratio for the CPB profile was found to be higher than that for the RBB profile, but lower than that for the SWB profile owing to the Cl level showed the highest value in the SWB profile. Interestingly, based on the Cl/EC ratio, Cl can also be used as a good marker for crop residue burning. The

emission of K in CPB as it showed the highest levels and could be a better indicator for differentiating these two profiles. The Cl/OC ratio (0.1) was relatively higher than the two biomass burning profiles, RBB and CPB. This indicates that the Cl level showed the highest value in the SWB profile and can be used as a good source marker for SWB profiles. The SWB profile was dominated by three elements such as Cl, S and K which accounted for 87.5%, 4.6% and

above source diagnostic ratios of chemical species can also be used as source indications and will help to distinguish all three types of biomass burning (RBB, SWB, and CPB) given in the present study. The CPB profile was dominated by Cl (68.2% of total elements) and K (24.8% of total elements) (Table S9, Fig. 6). The CPB source profile developed shows that Cl and K elements are good source indicators for the vegetative burning profiles. Crop residue burning is a major emitter of K, which accounted for $1.7 \pm 0.8\%$ of $PM_{2.5}$ mass (Table S9). As expected, the crustal elements (Si, Mg, and Na) were not found in the CPB profile. The trace elements were the lowest among all source profiles, accounting only for 1.3% of total elements. We conclude that the OC is a major species in this profile with a contribution of ~53.7% to the $PM_{2.5}$ total mass. OC1 showed the highest proportions as opposed to the lowest contributions shown by the OC4 and EC4, indicating that the most abundant source was the burning of biomass, meaning that the CPB profile was very well represented in this study. The CPB profile was also dominated by Cl and K.

4. Discussion

4.1. Chemical mass closure

Fig. 7 shows the results of the chemical mass closure for all source profiles. The PM mass was reconstructed on a source profile basis using the method described in Section 2.5. For CON, the order of fractions was as follows: MD (28.3%) > OM (25.8%) > ions (22.5%) > EC (13.8%) > other metals (9.5%) (Fig. 7). The CON was dominated by MD, OM, water-soluble ions and EC. This result indicated that good mass reconstruction and source markers were obtained for the CON. In addition, these fractions were higher than those reported in a previous study in India, in particular OM (9−12%) and EC (1−2%) (Patil et al., 2013). This may be associated with higher re-suspended soil dust and fuel combustion activities at the site in our study. Moreover, during the sampling, the construction site was at the initial phase of substructure construction including activities such as excavation and digging. The excavator, which includes heavy-duty diesel engines, were operational during the monitoring period, as described in Section 2.1. Other sources such as biomass burning by workers for heating/cooking at sites is another possible source, but such events occurred during the wind direction away from the sampling site (Fig. S3) and thus did not make any direct contributions to measured concentrations. PRD was dominated by the MD (76.3%), followed by OM (18.1%), ions (2.8%), other metals (1.9%) and EC (0.9%) (Fig. 7). The MD proportion is comparable with previous studies, e.g. 58−75% (Matawle et al., 2015), and 65−76% (Pervez et al., 2018), and relatively higher than the range (47%−56%) reported by Jiang et al. (2018). Interestingly, we found relatively higher OM (~18%) in PRD. This might be related to the traffic-related pollutants, including PAHs and possibly contributed by non-exhaust road materials such as asphalt (Khare at al., 2020), coal tar, tyre dust and organic-rich soil. However, further studies are needed to substantiate the non-exhaust component and the possible reasons for relatively high OM levels. In addition, the RBB, SWB, and CPB profiles were dominated by organic matter which accounted for 94.0%, 86.2% and 86.0%, respectively (Fig. 7). The percentages for other components (EC, ions, MD and other metals) accounted for ~ 6.0%, 13.8% and 13.9% of the mass for RBB, SWB and CPB profiles, respectively (Fig. 7). This indicated that the biomass, open solid waste and crop residue burning emissions were dominated by organic compounds. Previous studies reported similar results for OM emitted from roadside biomass, solid waste burning and crop residue burning (Bano et al., 2018; Barraza et al., 2020; Guo et al., 2017; Pandey et al., 2014). The OM proportion obtained in this study was relatively higher than
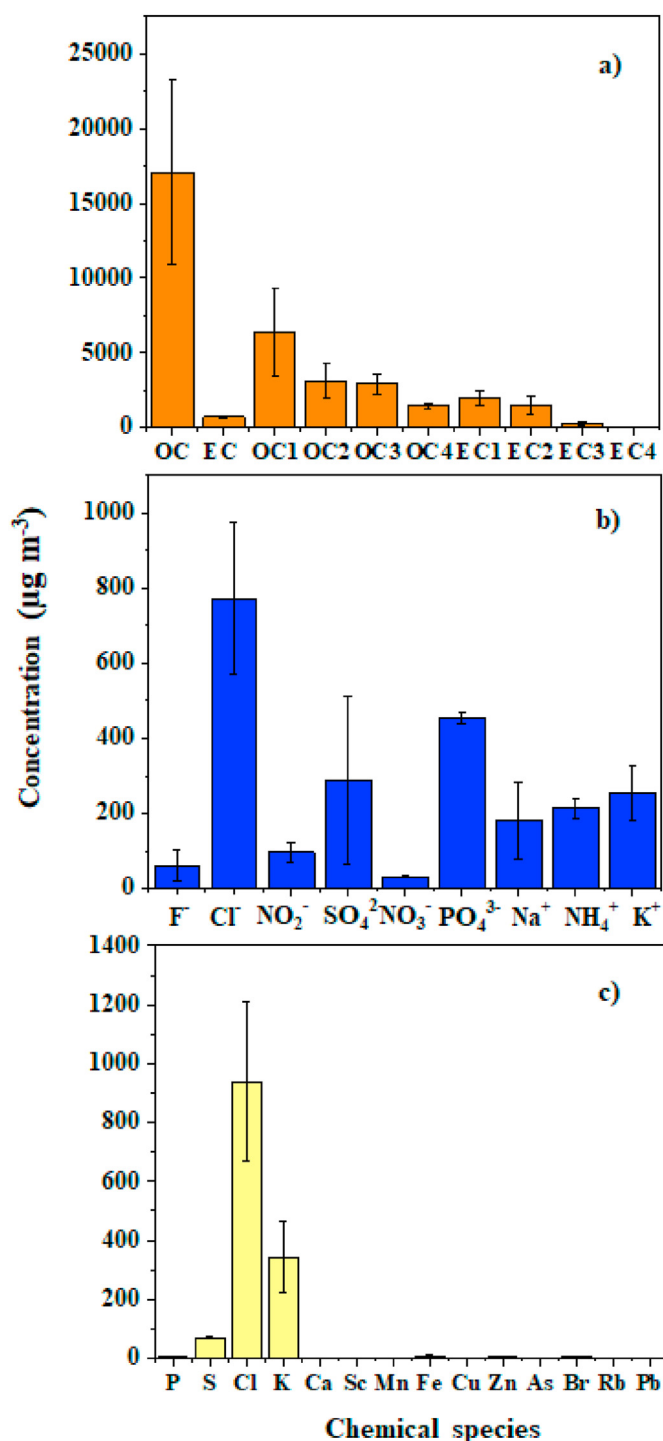
Fig. 6. Variability in mass concentrations ($\mu g\ m^{-3}$) of (a) carbonaceous species, (b) ions, and (c) elements for crop residue burning profile. The error bars represent the standard deviation for each of the species.

previous studies, for example, 69−88% (Bano et al., 2018) and 80−84% (Matawle et al., 2014) in India. Notably, the proportion of the above fractions of reconstructed PM mass were higher than that found in urban areas (Hama et al., 2018; Galindo et al., 2020; Kubelova et al., 2015). This indicated that good mass reconstruction and source markers were achieved for all developed source profiles. It can be concluded that OM, MD and ions were major components in CON. PRD was dominated by the ions and MD. OM was the most
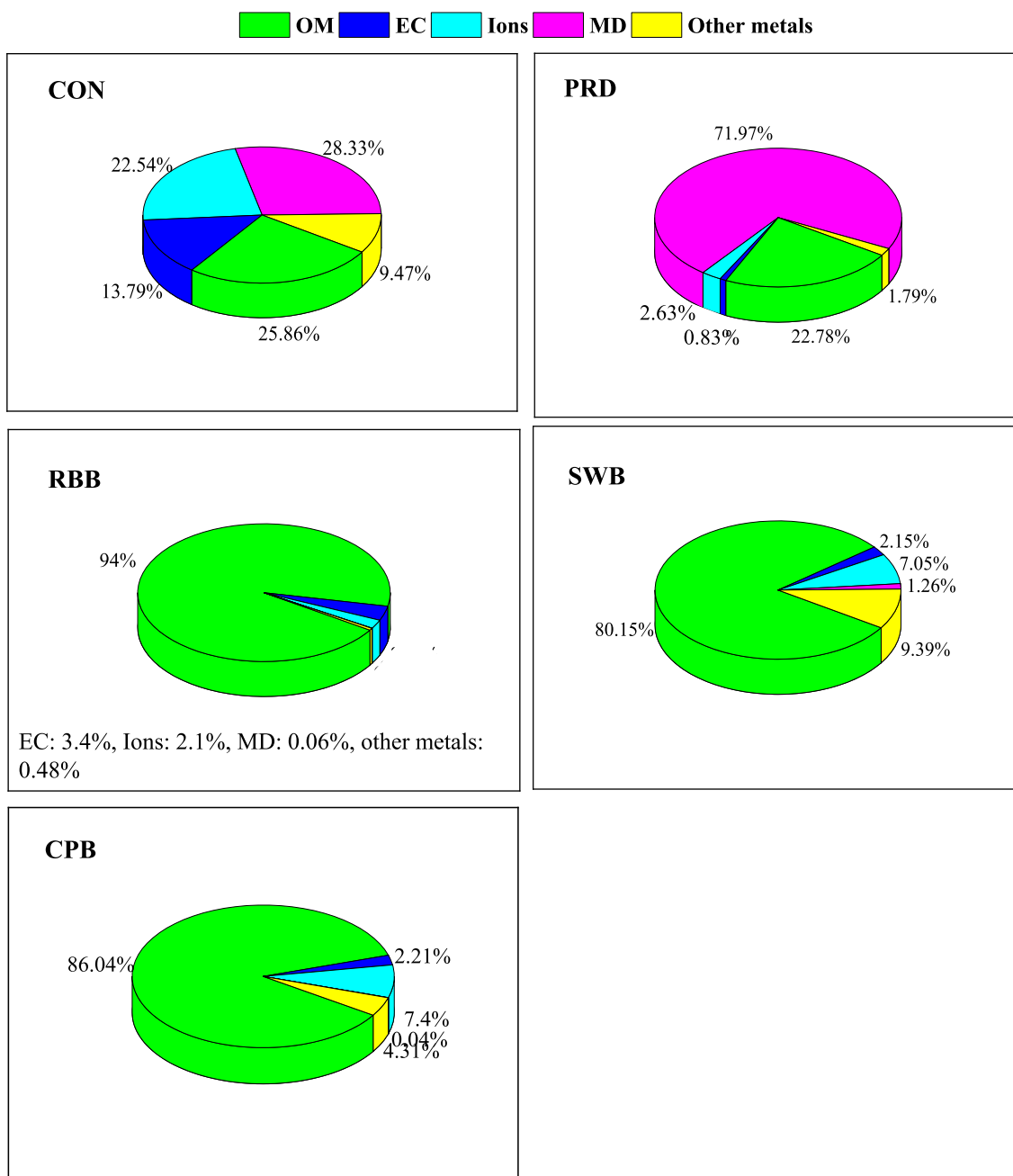
Fig. 7. Chemical mass closure of PM for all five source profiles. Four profiles (CON, RBB, SWB, and CPB) presented as $PM_{2.5}$, and the PRD presented PM_{10} fraction. OM: organic matter; EC: elemental carbon; Ions: all inorganic ions; MD: mineral dust; other metals: all metals which has not been used in the MD.

abundant species in all combustion profiles (RBB, SWB, and CPB). It is worth noting that some of the factors used in this section to calculate mass closure are derived from the literature and can be directly representative of the Indian situation. The source profiles developed in this work are representative of the current situation and source characteristics in Delhi and may be applied in quantifying the contribution of sources by receptor modelling, such as that using the CMB model.

4.2. Enrichment factor analysis for the CON and PRD profiles

Fig. 8 shows the EFs for crustal elements in CON and PRD profiles, computed using the approach described in Section 2.6. EFs are

used to assess anthropogenic contributions to the elements in CON and PRD profiles. It should be noted that calculation of EFs provides qualitative insight, because of the wide variation of elemental concentration of the upper crust at different locations (Samiksha et al., 2017). Notably, among all elements in both profiles, Ca was highly enriched with EFs of 4.1 and 5.0 for CON and PRD, respectively (Fig. 8). This indicated that both profiles represent construction activity and road dust emissions as both profiles were rich in Ca. The calculated EFs were generally lower and close to one for Si and Mg in both CON and PRD, indicating that crustal material was the main source. The calculated EFs were higher than one for other elements in both profiles, indicating that anthropogenic sources contributed. The EFs for all elements in PRD were higher than their
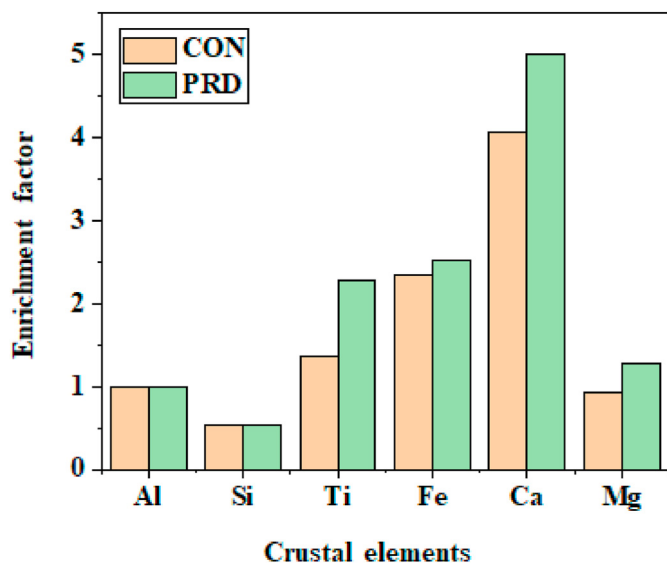
Fig. 8. Enrichment factors for the crustal elements in construction and paved road dust profiles.

corresponding values for CON. This observation suggests that the anthropogenic source contributions to PRD were higher than those in the CON profile.

4.3. Source markers

Table 4 shows the source markers for all source profiles. Values were calculated using the method described in Section 2.7. The six chemical species with the highest ratio values for total relative source profiles are considered representative source markers, and compared with previous studies (Bano et al., 2018; Chen et al., 2017; Kong et al., 2012; Matawle et al., 2014; Ni et al., 2017; Pervez et al., 2018; Watson et al., 2008; Wang et al., 2018). OC, EC, Na$^+$, NO$_3^-$, K and Si were identified as a source marker for CON in the current study (Table 4). This is slightly different from that reported

in previous studies (Kong et al., 2012; Matawle et al., 2015; Pervez et al., 2018). This may be related to the sampling location in previous studies. It should be noted that the source markers identified are very varied across previous studies due to the challenging nature of obtaining real construction signatures. OC, Si, Ca, Al, Fe and K were found to be representative chemical species for PRD. The source-specific tracers for PRD were similar to those reported in previous studies (Table 4). This indicates the chemical composition of road dust is dominated by crustal elements (Si, Ca, Al, Fe and K) in cities (Sun et al., 2019a). Six chemical species (OC, EC, SO$_4^{2-}$, NO$_3^-$, PO$_4^{3-}$ and Cl) were found to be source markers for RBB. They showed a high ratio (Eq. 10) values among all chemical species. RBB samples are dominated by OC followed by EC. OC, Cl, EC, PO$_4^{3-}$, NH$_4^+$ and S were identified as source markers for SWB. This is comparable to previous studies (Bano et al., 2018; Watson et al., 2008). Notably, we identified NH$_4^+$, PO$_4^{3-}$ and EC species in SWB which were not highlighted in previous studies (Bano et al., 2018; Matawle et al., 2014). This can be associated with the nature and type of materials burnt during sampling as very diverse materials (such as clothes, and plastics) were observed to have accumulated in the landfill and were burning on site. This is a typical behaviour of some cities in India and open burning of solid waste is a major contributor to air pollution in India (Kumar et al., 2015; Nagpure et al., 2015). Chemical species such as OC, Cl, EC, PO$_4^{3-}$, K and S were found as source markers for CPB. This is comparable with reported source markers in previous studies (Chen et al., 2017; Chow et al., 2004; Ni et al., 2017; Wang et al., 2020b). It can be noted that OC and Cl were the major chemical species found in the CPB profile. Crop residue burning in the open field, of which 18% (by weight) is contributed by India (Ravindra et al., 2019). Emissions from crop residue burning in the states of Punjab and Haryana (after harvesting by farmers in post-monsoon season) is frequently advected towards Delhi (Jethva et al., 2018; Ravindra et al., 2019, 2020; Shivani et al., 2019). New sets of source signatures for five different source profiles of Indian origin have been observed compared with those reported elsewhere (Table 4). Differences in source markers of PM$_{2.5}$ and PM$_{10}$ emissions from selected source profiles compared with those reported earlier (Table 4), are attributed to local factors and behaviours, highlighting the

Table 4
Source markers of PM for all source profiles.

Source profiles	Fraction of PM	Source signatures	References
CON	PM$_{2.5}$	OC, EC, Na$^+$, NO$_3^-$, K, and Si	This study
	PM$_{10-2.5}$	Al, Ca, Mg, NO$_3^-$, K, and Mg^{2+}	Pervez et al. (2018)
	PM$_{2.5}$	Zn, Na, Mo, Al, Mg2+, and Ca	Matawle et al. (2015)
	PM$_{10}$	Zn, Mg, V, Mg^{2+}, As, and NO$_3^-$	Kong et al. (2012)
	PM$_{2.5}$	Al, Si, K, Ca, and Fe	Watson et al. (2008)
PRD	PM$_{10}$	OC, Si, Ca, Al, Fe, and K	This study
	PM$_{10-2.5}$	Pb, Mg, Se, NO$_3^-$, Ca, and K	Pervez et al. (2018)
	PM$_{2.5}$	Na$^+$, SO$_4^{2-}$, As, F$^-$, Mg^{2+}, and Se	Matawle et al. (2015)
	PM$_{10}$	S, Zn, NO$_3^-$, Cl$^-$, Mg^{2+}, and NH$_4^+$	Kong et al. (2012)
	PM$_{2.5}$	Al, Si, K, Ca, and Fe	Watson et al. (2008)
RBB	PM$_{2.5}$	OC, EC, SO$_4^{2-}$, NO$_2^-$, PO$_4^{3-}$ and Cl	This study
	PM$_{10-2.5}$	As, Cr, K, NO$_3^-$, K$^+$, and EC	Bano et al. (2018)
	PM$_{10-2.1}$	OC, Cl-, K, and Na	Chen et al. (2017)
	PM$_{2.5}$	F$^-$, As, Mg^{2+}, Ca^{2+}, Cr, K$^+$	Matawle et al. (2014)
	PM$_{2.5}$	K, As	Andersen et al. (2007)
SWB	PM$_{2.5}$	OC, Cl, EC, PO$_4^{3-}$, NH$_4^+$ and S	This study
	PM$_{10-2.5}$	Cd, K, Mo, NO$_3^-$, K$^+$, and OC	Bano et al. (2018)
	PM$_{2.5}$	F$^-$, Co, Cd, Ca^{2+}, Na$^+$, and K$^+$	Matawle et al. (2014)
	PM$_{2.5}$	OC, EC, K$^+$, As, Pb, and Zn	Watson et al. (2008)
CPB	PM$_{2.5}$	OC, Cl, EC, PO$_4^{3-}$, K and S	This study
	PM$_{2.5}$	OC, Cl, Cl$^-$, EC, K, and K$^+$	Wang et al. (2020a, 2020b)
	PM$_{2.5}$	OC, K$^+$, K,	Chen et al. (2017)
	PM$_{2.5}$	OC, EC, Cl-, K$^+$, K, and Cl	Ni et al. (2017)
	PM$_{2.5}$	OC, K$^+$ and Na$^+$	Chow et al. (2004)

importance of development of region-specific source profiles to obtain precise results in receptor modelling. These profiles can be used in receptor model studies, to estimate the contribution of different sources to particulate mass concentrations observed within the Delhi and Haryana regions.

5. Conclusions and future outlook

We developed chemical source profiles of five principal PM sources in and around Delhi, based on three intensive field campaigns carried out in 2018. The key conclusions drawn from this work are as follows:

- The construction profile (CON) was dominated by OC, EC, Na^+, NO_3^- and SO_4^{2-}, and the most abundant elements were K, Si, Fe, Al, Na and Ca.
- The paved road dust profile (PRD) was dominated by OC, of which the major OC fractions were OC4 and OC3. We also found high levels of water-soluble ions such as PO_4^{3-}, SO_4^{2-} and Na^+. Overall, PRD was dominated by crustal elements and accounted for 91% of the total analysed elements in PRD. Si and Ca showed the highest fraction in PRD which accounted for 30% and 27% of total elements in road dust, respectively.
- The roadside biomass burning profile (RBB) was dominated by OC which accounted for 58.7% of $PM_{2.5}$ mass. The major ions were SO_4^{2-}, NO_2^-, PO_4^{3-} and Cl^- in the RBB profile. The most abundant metals were Cl, S and K which accounted for 88% of total elements.
- For the solid waste burning profile (SWB), OC was the most abundant species and accounted for 53.8% of $PM_{2.5}$ mass. OC1 showed the highest, followed by OC2, OC3 and OC4. EC1 showed the highest, followed by EC2, EC3, and EC4. The SWB profile also showed high Cl, S and K.
- For the crop residue burning profile (CPB), OC is a major species with a contribution of 53.7% to the $PM_{2.5}$ total mass. OC1 and EC1 showed the highest proportion within the OC and EC component, while OC4 and EC4 showed the lowest. The CPB profile also showed high Cl and K.
- For the CON source profile, the dominant fractions were MD (28.3%), followed by OM (25.8%), water-soluble ions (22.5%). PRD was dominated by MD (76.3%). In addition, RBB, SWB and CPB profiles were dominated by organic matter which accounted for 94%, 86.2% and 86.0% respectively.
- In the CON and PRD profiles, enrichment factors (EFs) of Si and Mg were lower or close to one, indicating that these elements originated from crustal material. In contrast, EFs for other elements were significantly higher than one, indicating that crustal material and anthropogenic sources were the main contributors.
- Six chemical species (OC, EC, Na^+, NO_3^-, K, and Si); (OC, Si, Ca, Al, Fe, and K); (OC, EC, SO_4^{2-}, NO_3^-, PO_4^{3-}, and Cl)); (OC, Cl, EC, PO_4^{3-}, NH_4^+ and S); and (OC, Cl, EC, PO_4^{3-}, K and S) were identified as source markers for CON, PRD, RBB, SWB and CPB profiles respectively.

The profiles developed and the associated new database are representative of current sources in Delhi. They may be instrumental in accurately estimating the contribution of different sources to PM through receptor modelling studies. Similar studies in different Indian cities and elsewhere are recommended to provide comparable databases that could also establish the extent to which source profiles can vary from city to city. Our source profile for the construction source is representative of substructure (i.e. below-ground construction), such as excavation of soil, which may vary for superstructure development (i.e. above-ground construction) activities. Thus, further studies are recommended to develop the source profile covering different phases of the construction process for a holistic assessment.

CRediT author statement

Sarkawt Hama: Formal analysis, Data Curation, Methodology, Writing - Original Draft, Investigation, Validation, Writing - review & editing. Prashant Kumar: Conceptualization, Funding acquisition, Writing - Original Draft, Resources, Supervision, Project Administration, Writing - review & editing. Mohammed S. Alam: Resources, Writing - review & editing. Daniel Rooney: Resources. William J. Bloss: Funding acquisition, Conceptualization, Writing - review & editing. Zongbo Shi: Writing - review & editing. Roy Harrison: Writing - review & editing. Leigh R. Crilley: Writing - review & editing. Mukesh Khare: Writing - review & editing. Sanjay Kumar Gupta: Writing - review & editing.

Declaration of competing interest

The authors declare that they have no known competing financial interests or personal relationships that could have appeared to influence the work reported in this paper.

Acknowledgements

Appendix A. Supplementary data

Supplementary data to this article can be found online at https://doi.org/10.1016/j.chemosphere.2021.129913.

References

AirMetrics, M.T., 2006. Operation Manual Version 5.0. Airmetrics TM, Eugene, Oregon. http://www.airmetrics.com/downloads.html.

Andersen, Z.J., Wahlin, P., Raaschou-Nielsen, O., Scheike, T., Loft, S., 2007. Ambient particle source apportionment and daily hospital admissions among children and elderly in Copenhagen. J. Expo. Sci. Environ. Epidemiol. 17, 625−636.

Atkinson, R.W., Mills, I.C., Walton, H.A., Anderson, H.R., 2015. Fine particle components and health—a systematic review and meta-analysis of epidemiological time series studies of daily mortality and hospital admissions. J. Expo. Sci. Environ. Epidemiol. 25, 208−214.

Bano, S., Pervez, S., Chow, J.C., Matawle, J.L., Watson, J.G., Sahu, R.K., Srivastava, A., Tiwari, S., Pervez, Y.F., Deb, M.K., 2018. Coarse particle ($PM_{10−2.5}$) source profiles for emissions from domestic cooking and industrial process in Central India. Sci. Total Environ. 627, 1137−1145.

Barraza, F., Uzu, G., Jaffrezo, J.L., Schreck, E., Budzinski, H., Le Menach, K., Dévier, M.H., Guyard, H., Calas, A., Perez, M.I., Villacreces, L.A., 2020. Contrasts in chemical composition and oxidative potential in PM10 near flares in oil extraction and refining areas in Ecuador. Atmos. Environ. 223, 117302.

Cavalli, F., Viana, M., Yttri, K.E., Genberg, J., Putaud, J.-P., 2010. Toward a standardised thermal-optical protocol for measuring atmospheric organic and elemental carbon: the EUSAAR protocol. Atmos. Meas. Tech. 3, 79−89.

Cesari, D., Contini, D., Genga, A., Siciliano, M., Elefante, C., Baglivi, F., Daniele, L., 2012. Analysis of raw soils and their re-suspended PM_{10} fractions: characterisation of source profiles and enrichment factors. Appl. Geochem. 27, 1238−1246.

Chan, Y.C., Simpson, R.W., McTainsh, G.H., Vowles, P.D., Cohen, D.D., Bailey, G.M., 1997. Characterisation of chemical species in $PM_{2.5}$ and PM_{10} aerosols in Brisbane, Australia. Atmos. Environ. 31, 3773−3785.

Chen, S.J., Hsieh, L.T., Chiu, S.C., 2003. Emission of polycyclic aromatic hydrocarbons from animal carcass incinerators. Sci. Total Environ. 313, 61−76.

Chen, Y., Tian, C., Feng, Y., Zhi, G., Li, J., Zhang, G., 2015. Measurements of emission

factors of PM2. 5, OC, EC, and BC for household stoves of coal combustion in China. Atmos. Environ. 109, 190−196.

Chen, P., Wang, T., Dong, M., Kasoar, M., Han, Y., Xie, M., Li, S., Zhuang, B., Li, M., Huang, T., 2017. Characterization of major natural and anthropogenic source profiles for size-fractionated PM in Yangtze River Delta. Sci. Total Environ. 598, 135−145.

Cheng, Y., Engling, G., He, K.-B., Duan, F.-K., Ma, Y.-L., Du, Z.-Y., Liu, J.-M., Zheng, M., Weber, R.J., 2013. Biomass burning contribution to Beijing aerosol. Atmos. Chem. Phys. 13, 7765−7781.

Chow, J.C., Watson, J.G., 1998. Guideline on Speciated Particulate Monitoring. Report prepared for US Environmental Protection Agency, Research Triangle Park, NC (by Desert Research Institute, Reno, NV).

Chow, J.C., Watson, J.G., Kuhns, H., Etyemezian, V., Lowenthal, D.H., Crow, D., Kohl, S.D., Engelbrecht, J.P., Green, M.C., 2004. Source profiles for industrial, mobile, and area sources in the big bend regional aerosol visibility and observational study. Chemosphere 54, 185−208.

Chow, J.C., Lowenthal, D.H., Chen, L.W.A., Wang, X., Watson, J.G., 2015. Mass reconstruction methods for PM$_{2.5}$: a review. Aai Qual. Atmos. Hlth. 8, 243−263.

Cohen, A.J., Brauer, M., Burnett, R., Anderson, H.R., Frostad, J., Estep, K., Balakrishnan, K., Brunekreef, B., Dandona, L., Dandona, R., Feigin, V., 2017. Estimates and 25-year trends of the global burden of disease attributable to ambient air pollution: an analysis of data from the Global Burden of Diseases Study 2015. Lancet 389, 1907−1918.

Conibear, L., Butt, E.W., Knote, C., Arnold, S.R., Spracklen, D.V., 2018. Residential energy use emissions dominate health impacts from exposure to ambient particulate matter in India. Nat. Commun. 9, 1−9.

Crilley, L.R., Lucarelli, F., Bloss, W.J., Harrison, R.M., Beddows, D.C., Calzolai, G., Nava, S., Valli, G., Bernardoni, V., Vecchi, R., 2017. Source apportionment of fine and coarse particles at a roadside and urban background site in London during the 2012 summer ClearfLo campaign. Environ. Pollut. 220, 766−778.

Das, R., Khezri, B., Srivastava, B., Datta, S., Sikdar, P.K., Webster, R.D., Wang, X., 2015. Trace element composition of PM2.5 and PM10 from Kolkata−a heavily polluted Indian metropolis. Atmos. Pollut. Res. 6, 742−750.

Duan, J., Tan, J., 2013. Atmospheric heavy metals and arsenic in China: situation, sources and control policies. Atmos. Environ. 74, 93−101.

Galindo, N., Yubero, E., Clemente, Á., Nicolás, J.F., Varea, M., Crespo, J., 2020. PM events and changes in the chemical composition of urban aerosols: a case study in the western Mediterranean. Chemosphere 244, 125520.

Gao, S., Xu, B., Dong, X., Zheng, X., Wan, X., Kang, S., Song, Q., Kawamura, K., Cong, Z., 2018. Biomass-burning derived aromatic acids in NIST standard reference material 1649b and the environmental implications. Atmos. Environ. 185, 180−185.

Guo, H., Kota, S.H., Sahu, S.K., Hu, J., Ying, Q., Gao, A., Zhang, H., 2017. Source apportionment of PM$_{2.5}$ in North India using source-oriented air quality models. Environ. Pollut. 231, 426−436.

Hama, S.M., Cordell, R.L., Staelens, J., Mooibroek, D., Monks, P.S., 2018. Chemical composition and source identification of PM$_{10}$ in five North Western European cities. Atmos. Res. 214, 135−149.

Hama, S.M., Kumar, P., Harrison, R.M., Bloss, W.J., Khare, M., Mishra, S., Namdeo, A., Sokhi, R., Goodman, P., Sharma, C., 2020. Four-year assessment of ambient particulate matter and trace gases in the Delhi-NCR region of India. Sustain. Cities Soc. 54, 102003.

Han, Y.M., Chen, L.W., Huang, R.J., Chow, J.C., Watson, J.G., Ni, H.Y., Liu, S.X., Fung, K.K., Shen, Z.X., Wei, C., Wang, Q.Y., 2016. Carbonaceous aerosols in megacity Xi'an, China: implications of thermal/optical protocols comparison. Atmos. Environ. 132, 58−68.

Harris, E., Sinha, B., Van Pinxteren, D., Tilgner, A., Fomba, K.W., Schneider, J., Roth, A., Gnauk, T., Fahlbusch, B., Mertes, S., Lee, T., 2013. Enhanced role of transition metal ion catalysis during in-cloud oxidation of SO$_2$. Science 340, 727−730.

Heal, M.R., Kumar, P., Harrison, R.M., 2012. Particles, air quality, policy and health. Chem. Soc. Rev. 41, 6606−6630.

Ho, K.F., Lee, S.C., Chow, J.C., Watson, J.G., 2003. Characterization of PM$_{10}$ and PM$_{2.5}$ source profiles for fugitive dust in Hong Kong. Atmos. Environ. 37, 1023−1032.

Huang, B.F., Chang, Y.C., Han, A.L., Hsu, H.T., 2018. Metal composition of ambient PM$_{2.5}$ influences the pulmonary function of schoolchildren: a case study of school located nearby of an electric arc furnace factory. Toxicol. Ind. Health 34, 253−261.

Huang, J., Pan, X., Guo, X., Li, G., 2018. Health impact of China's Air Pollution Prevention and Control Action Plan: an analysis of national air quality monitoring and mortality data. Lancet Planet. Health 2, 313−323.

Izhar, S., Goel, A., Chakraborty, A., Gupta, T., 2016. Annual trends in occurrence of submicron particles in ambient air and health risk posed by particle bound metals. Chemosphere 146, 582−590.

Jain, S., Sharma, S.K., Vijayan, N., Mandal, T.K., 2020. Seasonal characteristics of aerosols (PM$_{2.5}$ and PM$_{10}$) and their source apportionment using PMF: a four-year study over Delhi, India. Environ. Pollut. 262, 114337.

Jethva, H.T., Chand, D., Torres, O., Gupta, P., Lyapustin, A., Patadia, F., 2018. Agricultural burning and air quality over northern India: a synergistic analysis using NASA's A-train satellite data and ground measurements. Aerosol and Air Quality Research 18, 1756−1773.

Jiang, N., Dong, Z., Xu, Y., Yu, F., Yin, S., Zhang, R., Tang, X., 2018. Characterization of PM10 and PM2.5 source profiles of fugitive dust in Zhengzhou, China. Aerosol Air Qual. Res. 18, 314−329.

Kaskaoutis, D.G., Kumar, S., Sharma, D., Singh, R.P., Kharol, S.K., Sharma, M., Singh, A.K., Singh, S., Singh, A., Singh, D., 2014. Effects of crop residue burning on aerosol properties, plume characteristics, and long-range transport over

northern India. J. Geophys. Res. Atmos. 119, 5424−5444.

Khare, P., Machesky, J., Soto, R., He, M., Presto, A.A., Gentner, D.R., 2020. Asphalt-related emissions are a major missing nontraditional source of secondary organic aerosol precursors. Science Advances 6, eabb9785.

Kim, H., Zhang, Q., Heo, J., 2018. Influence of intense secondary aerosol formation and long-range transport on aerosol chemistry and properties in the Seoul Metropolitan Area during spring time: results from KORUS-AQ. Atmos. Chem. Phys. 18, 7149−7168.

Kong, S., Lu, B., Ji, Y., Bai, Z., Xu, Y., Liu, Y., Jiang, H., 2012. Distribution and sources of polycyclic aromatic hydrocarbons in size-differentiated re-suspended dust on building surfaces in an oilfield city, China. Atmos. Environ. 55, 7−16.

Kubelová, L., Vodička, P., Schwarz, J., Cusack, M., Makeš, O., Ondráček, J., Ždímal, V., 2015. A study of summer and winter highly time-resolved submicron aerosol composition measured at a suburban site in Prague. Atmos. Environ. 118, 45−57.

Kumar, S., Raman, R.S., 2020. Source apportionment of fine particulate matter over a National Park in Central India. Sci. Total Environ. 720, 137511.

Kumar, P., Jain, S., Gurjar, B.R., Sharma, P., Khare, M., Morawska, L., Britter, R., 2013. New directions: can a "blue sky" return to Indian megacities? Atmos. Environ. 71, 198−201.

Kumar, R., Barth, M.C., Madronich, S., Naja, M., Carmichael, G.R., Pfister, G.G., Knote, C., Brasseur, G.P., Ojha, N., Sarangi, T., 2014. Effects of dust aerosols on tropospheric chemistry during a typical pre-monsoon season dust storm in northern India. Atmos. Chem. Phys. 14, 6813−6834.

Kumar, P., Khare, M., Harrison, R.M., Bloss, W.J., Lewis, A., Coe, H., Morawska, L., 2015. New directions: air pollution challenges for developing megacities like Delhi. Atmos. Environ. 122, 657−661.

Kumar, P., Gulia, S., Harrison, R.M., Khare, M., 2017. The influence of odd−even car trial on fine and coarse particles in Delhi. Environ. Pollut. 225, 20−30.

Kumar, P., Hama, S., Omidvarborna, H., Sharma, A., Sahani, J., Abhijith, K.V., Debele, S.E., Zavala-Reyes, J.C., Barwise, Y., Tiwari, A., 2020. Temporary reduction in fine particulate matter due to 'anthropogenic emissions switch-off' during COVID-19 lockdown in Indian cities. Sustainable Cities and Society 62, 102382.

Landrigan, P.J., Fuller, R., Acosta, N.J., Adeyi, O., Arnold, R., Baldé, A.B., Bertollini, R., Bose-O'Reilly, S., Boufford, J.I., Breysse, P.N., Chiles, T., 2018. The Lancet Commission on pollution and health. Lancet 391, 462−512.

Malav, L.C., Yadav, K.K., Gupta, N., Kumar, S., Sharma, G.K., Krishnan, S., Rezania, S., Kamyab, H., Pham, Q.B., Yadav, S., Bhattacharyya, S., 2020. A review on municipal solid waste as a renewable source for waste-to-energy project in India: current practices, challenges, and future opportunities. J. Clean. Prod. 277, 123227.

Marcazzan, G.M., Vaccaro, S., Valli, G., Vecchi, R., 2001. Characterisation of PM$_{10}$ and PM$_{2.5}$ particulate matter in the ambient air of Milan (Italy). Atmos. Environ. 35, 4639−4650.

Matawle, J., Pervez, S., Dewangan, S., Tiwari, S., Bisht, D.S., Pervez, Y.F., 2014. PM$_{2.5}$ chemical source profiles of emissions resulting from industrial and domestic burning activities in India. Aerosol Air Qual. Res. 14, 2051−2066.

Matawle, J.L., Pervez, S., Dewangan, S., Shrivastava, A., Tiwari, S., Pant, P., Deb, M.K., Pervez, Y., 2015. Characterization of PM$_{2.5}$ source profiles for traffic and dust sources in Raipur, India. Aerosol Air Qual. Res 15, 2537−2548.

Meng, Q., Richmond-Bryant, J., Lu, S.E., Buckley, B., Welsh, W.J., Whitsel, E.A., Hanna, A., Yeatts, K.B., Warren, J., Herring, A.H., Xiu, A., 2013. Cardiovascular outcomes and the physical and chemical properties of metal ions found in particulate matter air pollution: a QICAR study. Environ. Health Perspect. 121, 558−564.

Mitra, A.P., Morawska, L., Sharma, C., Zhang, J., 2002. Chapter two: methodologies for characterisation of combustion sources and for quantification of their emissions. Chemosphere 49, 903−922.

Moreno, T., Merolla, L., Gibbons, W., Greenwell, L., Jones, T., Richards, R., 2004. Variations in the source, metal content and bioreactivity of technogenic aerosols: a case study from Port Talbot, Wales, UK. Sci. Total Environ. 333, 59−73.

Nagpure, A.S., Ramaswami, A., Russell, A., 2015. Characterizing the spatial and temporal patterns of open burning of municipal solid waste (MSW) in Indian cities. Environ. Sci. Technol. 49, 12904−12912.

Ni, H., Tian, J., Wang, X., Wang, Q., Han, Y., Cao, J., Long, X., Chen, L.W.A., Chow, J.C., Watson, J.G., Huang, R.J., 2017. PM$_{2.5}$ emissions and source profiles from open burning of crop residues. Atmos. Environ. 169, 229−237.

Pandey, A., Sadavarte, P., Rao, A.B., Venkataraman, C., 2014. Trends in multi-pollutant emissions from a technology-linked inventory for India: II. Residential, agricultural and informal industry sectors. Atmos. Environ. 99, 341−352.

Pant, P., Harrison, R.M., 2012. Critical review of receptor modelling for particulate matter: a case study of India. Atmos. Environ. 49, 1−12.

Pant, P., Baker, S.J., Shukla, A., Maikawa, C., Pollitt, K.J.G., Harrison, R.M., 2015. The PM$_{10}$ fraction of road dust in the UK and India: characterization, source profiles and oxidative potential. Sci. Total Environ. 530, 445−452.

Patil, R.S., Kumar, R., Menon, R., Shah, M.K., Sethi, V., 2013. Development of particulate matter speciation profiles for major sources in six cities in India. Atmos. Res. 132, 1−11.

Pernigotti, D., Belis, C.A., Spano, L., 2016. SPECIEUROPE: the European data base for PM source profiles. Atmos. Pollut. Res. 7, 307−314.

Pervez, S., Bano, S., Watson, J.G., Chow, J.C., Matawle, J.L., Shrivastava, A., Tiwari, S., Pervez, Y.F., 2018. Source profiles for PM10-2.5 resuspended dust and vehicle exhaust emissions in central India. Aerosol Air Qual. Res. 18, 1660−1672.

Pipalatkar, P., Khaparde, V.V., Gajghate, D.G., Bawase, M.A., 2014. Source apportionment of PM$_{2.5}$ using a CMB model for a centrally located Indian city. Aerosol

Air Qual. Res 14, 1089–1099.

Rai, P., Furger, M., El Haddad, I., Kumar, V., Wang, L., Singh, A., Dixit, K., Bhattu, D., Petit, J.E., Ganguly, D., Rastogi, N., 2020. Real-time measurement and source apportionment of elements in Delhi's atmosphere. Sci. Total Environ. 742, 140332.

Ravindra, K., Singh, T., Mor, S., 2019. Emissions of air pollutants from primary crop residue burning in India and their mitigation strategies for cleaner emissions. J. Clean. Prod. 208, 261–273.

Ravindra, K., Singh, T., Pandey, V., Mor, S., 2020. Air pollution trend in Chandigarh city situated in Indo-Gangetic Plains: understanding seasonality and impact of mitigation strategies. Sci. Total Environ. 729, 138717.

Rees, S.L., Robinson, A.L., Khlystov, A., Stanier, C.O., Pandis, S.N., 2004. Mass balance closure and the federal reference method for PM2.5 in pittsburgh, Pennsylvania. Atmos. Environ. 38, 3305–3318.

Samiksha, S., Raman, R.S., Nirmalkar, J., Kumar, S., Sirvaiya, R., 2017. PM10 and PM2.5 chemical source profiles with optical attenuation and health risk indicators of paved and unpaved road dust in Bhopal, India. Environ. Pollut. 222, 477–485.

Schnell, J.L., Naik, V., Horowitz, L.W., Paulot, F., Mao, J., Ginoux, P., Zhao, M., Ram, K., 2018. Exploring the relationship between surface PM2.5 and meteorology in Northern India. Atmos. Chem. Phys. 18, 10157–10175.

Shen, Z., Sun, J., Cao, J., Zhang, L., Zhang, Q., Lei, Y., Gao, J., Huang, R.J., Liu, S., Huang, Y., Zhu, C., 2016. Chemical profiles of urban fugitive dust PM2.5 samples in Northern Chinese cities. Sci. Total Environ. 569, 619–626.

Shivani Gadi, R., Sharma, S.K., Mandal, T.K., 2019. Seasonal variation, source apportionment and source attributed health risk of fine carbonaceous aerosols over National Capital Region, India. Chemosphere 237, 124500.

Shukla, K., Kumar, P., Mann, G.S., Khare, M., 2020. Mapping spatial distribution of particulate matter using Kriging and Inverse Distance Weighting at supersites of megacity Delhi. Sustainable Cities and Society 54, 101997.

Singh, A.K., Singh, M., 2006. Lead decline in the Indian environment resulting from the petrol-lead phase-out programme. Sci. Total Environ. 368, 686–694.

Squizzato, S., Masiol, M., Brunelli, A., Pistollato, S., Tarabotti, E., Rampazzo, G., Pavoni, B., 2013. Factors determining the formation of secondary inorganic aerosol: a case study in the Po Valley (Italy). Atmos. Chem. Phys. 13, 1927–1939.

Sun, J., Shen, Z., Zhang, L., Lei, Y., Gong, X., Zhang, Q., Zhang, T., Xu, H., Cui, S., Wang, Q., Cao, J., 2019a. Chemical source profiles of urban fugitive dust PM2.5 samples from 21 cities across China. Sci. Total Environ. 649, 1045–1053.

Sun, J., Shen, Z., Zhang, Y., Zhang, Q., Lei, Y., Huang, Y., Niu, X., Xu, H., Cao, J., Ho, S.S.H., Li, X., 2019b. Characterization of PM2.5 source profiles from typical biomass burning of maize straw, wheat straw, wood branch, and their processed products (briquette and charcoal) in China. Atmos. Environ. 205, 36–45.

Tchounwou, P.B., Yedjou, C.G., Patlolla, A.K., Sutton, D.J., 2012. Heavy metal toxicity and the environment. Molecular, Clinical and Environmental Toxicology 101, 133–164.

Thepnuan, D., Chantara, S., Lee, C.T., Lin, N.H., Tsai, Y.I., 2019. Molecular markers for biomass burning associated with the characterization of PM2.5 and component sources during dry season haze episodes in Upper South East Asia. Sci. Total Environ. 658, 708–722.

van der Gon, H.A.C., Bergström, R., Fountoukis, C., Johansson, C., Pandis, S.N., Simpson, D., Visschedijk, A.J., 2015. Particulate emissions from residential wood combustion in Europe revised estimates and an evaluation. Atmos. Chem. Phys. 15, 6503–6519.

Vicente, E.D., Alves, C.A., 2018. An overview of particulate emissions from residential biomass combustion. Atmos. Res. 199, 159–185.

Wang, G., Zhang, F., Peng, J., Duan, L., Ji, Y., Marrero-Ortiz, W., Wang, J., Li, J., Wu, C., Cao, C., Wang, Y., 2018. Particle acidity and sulfate production during severe haze events in China cannot be reliably inferred by assuming a mixture of inorganic salts. Atmos. Chem. Phys. 18, 10123–10132.

Wang, J., Niu, X., Sun, J., Zhang, Y., Zhang, T., Shen, Z., Zhang, Q., Xu, H., Li, X., Zhang, R., 2020a. Source profiles of PM2.5 emitted from four typical open burning sources and its cytotoxicity to vascular smooth muscle cells. Sci. Total Environ. 715, 136949.

Wang, Q., Wang, L., Li, X., Xin, J., Liu, Z., Sun, Y., Liu, J., Zhang, Y., Du, W., Jin, X., Zhang, T., 2020b. Emission characteristics of size distribution, chemical composition and light absorption of particles from field-scale crop residue burning in Northeast China. Sci. Total Environ. 710, 136304.

Watson, J.G., Chow, J.C., 2001. Source characterization of major emission sources in the Imperial and Mexicali Valleys along the US/Mexico border. Sci. Total Environ. 276, 33–47.

Watson, J.G., Chow, J.C., Frazier, C.A., 1999. X-ray fluorescence analysis of ambient air samples. Elemental analysis of airborne particles 1, 67–96.

Watson, J.G., Chow, J.C., Houck, J.E., 2001. PM2.5 chemical source profiles for vehicle exhaust, vegetative burning, geological material, and coal burning in Northwestern Colorado during 1995. Chemosphere 43, 1141–1151.

Watson, J.G., Antony Chen, L.W., Chow, J.C., Doraiswamy, P., Lowenthal, D.H., 2008. Source apportionment: findings from the US supersites program. J. Air Waste Manage. 58, 265–288.

Wedepohl, K.H., 1995. The composition of the continental crust. Geochem. Cosmochim. Acta 59, 1217–1232.

WHO, 2018. World Health Organization, 2018. WHO global ambient air quality database (update 2018). Available: https://www.who.int/airpollution/data/cities/en/ (accessed 30th September 2020).

WPR, 2020. World population review. Population by city 2020. https://worldpopulationreview.com/world-cities/ (accessed 30th September, 2020).

Xu, H.M., Cao, J.J., Ho, K.F., Ding, H., Han, Y.M., Wang, G.H., Chow, J.C., Watson, J.G., Khol, S., Qiang, J., Li, W.T., 2012. Lead concentrations in fine particulate matter after the phasing out of leaded gasoline in Xi'an, China. Atmos. Environ. 46, 217–224.

Yang, H.H., Lai, S.O., Hsieh, L.T., Hsueh, H.J., Chi, T.W., 2002. Profiles of PAH emission from steel and iron industries. Chemosphere 48, 1061–1074.

Yatkin, S., Bayram, A., 2008. Determination of major natural and anthropogenic source profiles for particulate matter and trace elements in Izmir, Turkey. Chemosphere 71, 685–696.

Yu, H., Zhao, X., Wang, J., Yin, B., Geng, C., Wang, X., Gu, C., Huang, L., Yang, W., Bai, Z., 2020. Chemical characteristics of road dust PM2.5 fraction in oasis cities at the margin of Tarim Basin. J. Environ. Sci. 95, 217–224.

Zhang, H., Wang, S., Hao, J., Wan, L., Jiang, J., Zhang, M., Mestl, H.E., Alnes, L.W., Aunan, K., Mellouki, A.W., 2012. Chemical and size characterization of particles emitted from the burning of coal and wood in rural households in Guizhou, China. Atmos. Environ. 51, 94–99.

Zhang, Q., Shen, Z., Cao, J., Ho, K., Zhang, R., Bie, Z., Chang, H., Liu, S., 2014. Chemical profiles of urban fugitive dust over Xi'an in the south margin of the Loess Plateau, China. Atmospheric Pollution Research 5, 421–430.